Geologic Time Scale 2020

Volume 1

Felix M. Gradstein
James G. Ogg
Mark D. Schmitz
Gabi M. Ogg

ELSEVIER

Elsevier
Radarweg 29, PO Box 211, 1000 AE Amsterdam, Netherlands
The Boulevard, Langford Lane, Kidlington, Oxford OX5 1GB, United Kingdom
50 Hampshire Street, 5th Floor, Cambridge, MA 02139, United States

Copyright © 2020, Felix M. Gradstein, James G. Ogg, Mark D. Schmitz and Gabi M. Ogg. Published by Elsevier BV. All rights reserved.

No part of this publication may be reproduced or transmitted in any form or by any means, electronic or mechanical, including photocopying, recording, or any information storage and retrieval system, without permission in writing from the publisher. Details on how to seek permission, further information about the Publisher's permissions policies and our arrangements with organizations such as the Copyright Clearance Center and the Copyright Licensing Agency, can be found at our website: www.elsevier.com/permissions.

This book and the individual contributions contained in it are protected under copyright by the Publisher (other than as may be noted herein).

Notices
Knowledge and best practice in this field are constantly changing. As new research and experience broaden our understanding, changes in research methods, professional practices, or medical treatment may become necessary.

Practitioners and researchers must always rely on their own experience and knowledge in evaluating and using any information, methods, compounds, or experiments described herein. In using such information or methods they should be mindful of their own safety and the safety of others, including parties for whom they have a professional responsibility.

To the fullest extent of the law, neither the Publisher nor the authors, contributors, or editors, assume any liability for any injury and/or damage to persons or property as a matter of products liability, negligence or otherwise, or from any use or operation of any methods, products, instructions, or ideas contained in the material herein.

British Library Cataloguing-in-Publication Data
A catalogue record for this book is available from the British Library

Library of Congress Cataloging-in-Publication Data
A catalog record for this book is available from the Library of Congress

This Volume (1) ISBN: 978-0-12-824362-6
Volume 2 ISBN: 978-0-12-824363-3
Set ISBN: 978-0-12-824360-2

For Information on all Elsevier publications
visit our website at https://www.elsevier.com/books-and-journals

Front cover of Volume 1: Toarcian boundary stratotype section, Peniche, Portugal. Photograph by F.M. Gradstein.

Publisher: Candice Janco
Acquisitions Editor: Amy Shapiro
Editorial Project Manager: Susan Ikeda
Production Project Manager: Kiruthika Govindaraju
Cover Designer: Mark Rogers

Typeset by MPS Limited, Chennai, India

Working together to grow libraries in developing countries
www.elsevier.com • www.bookaid.org

A. Paytan, W. Yao, K.L. Faul and E.T. Gray

Chapter 9

Sulfur Isotope Stratigraphy

Chapter outline

Abstract

The sulfur isotopic composition of dissolved sulfate in seawater has varied through time. Distinct variations and relatively high rates of change characterize certain time intervals. This allows for dating and correlation of sediments using sulfur isotopes. The variation in sulfur isotopes and the potential stratigraphic resolution of this isotope system is discussed and graphically displayed. New data are used to refine the previously published (Geologic Time Scale 2012) for the Paleocene and Eocene.

9.1 Introduction

Sulfur isotope biogeochemistry has broad applications to geological, biological, and environmental studies. Sulfur is an important constituent of the Earth's lithosphere, biosphere, hydrosphere, and atmosphere and occurs as a major constituent or in trace amounts in various components of the Earth system. Many of the characteristics of sulfur isotope geochemistry are analogous to those of carbon and nitrogen, as all three elements occur in reduced and oxidized forms, and undergo an oxidation state change as a result of biological processes.

Sulfur as sulfate (SO_4^{2-}) is the second most abundant anion in modern seawater with an average present-day concentration of 28 mmol/kg. It has a conservative distribution with uniform SO_4^{2-}/salinity ratios in the open ocean and a very long residence time of close to 10 million years (Chiba and Sakai, 1985; Berner and Berner, 1987). Because of the large pool of sulfate in the ocean, it is expected that the rate of change in either concentration or isotopic composition of sulfate will be small, thus reducing the utility of this isotope system as a viable tool for stratigraphic correlation or dating.

However, as seen in Figs. 9.1–9.4, the isotopic record shows distinct variations through time, and at certain intervals, the rate of change and the unique features of the record may yield a reliable numerical age. The features in the record can also be used to correlate between stratigraphic sections and sequences. This is particularly important for sequences dominated by evaporites, where fossils are not abundant or have a restricted distribution range, paramagnetic minerals are rare, and other stratigraphic tools (e.g., oxygen isotopes in carbonates) cannot be utilized.

While the potential for the utility of sulfur isotope stratigraphy exists, this system has not been broadly applied. The examples for the application of S isotopes for stratigraphic correlations predominantly focus on the Neoproterozoic and often employ other methods of correlation such as $^{87}Sr/^{86}Sr$ and $\delta^{13}C$ as well (Misi et al., 2007; Pokrovskii et al., 2006; Walter et al., 2000; Hurtgen et al., 2002; Planavsky et al., 2012; Scott et al., 2014).

It is important to note that the method works only for marine minerals containing sulfate. Moreover, it is crucial that the integrity of the record be confirmed to insure the pristine nature of the record and lack of postdepositional alteration (Kampschulte and Strauss, 2004; Crockford et al., 2019). In the application of sulfur isotopes, it is assumed that the oceans are homogeneous with respect to

Geologic Time Scale 2020. DOI: https://doi.org/10.1016/B978-0-12-824360-2.00009-7
© 2020 Elsevier B.V. All rights reserved.

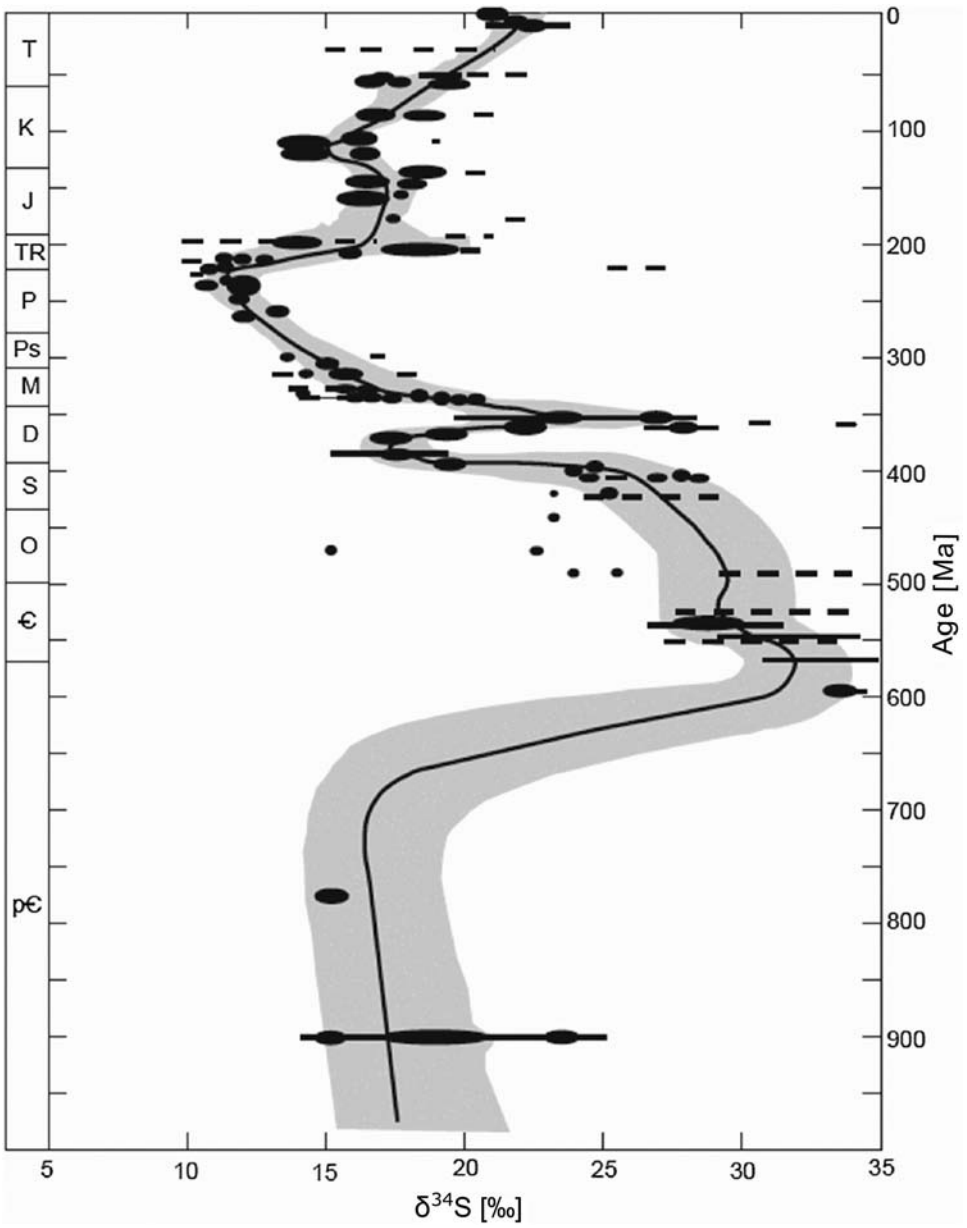

FIGURE 9.1 Evaporite records (Claypool et al., 1980). Solid lines represent data from Claypool et al. and data he compiled from the literature plotted at their most probable age. Dashed lines show the range of all available few analyses for each time interval. The heavy line is the best estimate of $\delta^{34}S$ of the ocean. The shaded area is the uncertainty related to the curve.

sulfur isotopes of dissolved sulfate and that they always were so. As noted, previously, uniformity is expected because of the long residence time of sulfate in the ocean (millions of years) compared to the oceanic mixing time (thousands of years) and because of the high concentration of sulfate in seawater compared to the concentration in major input sources of sulfur to the ocean (rivers, hydrothermal activity, and volcanic activity). Indeed, in the present-day ocean, seawater maintains constant sulfur isotopic composition (at an analytical precision of ~0.2‰) until it is diluted to salinities well below those supportive of fully marine fauna (Crockford et al., 2019) invalidating this assumption and limiting the utility of sulfur isotopes for stratigraphic correlation during such time intervals. The main limitation to the broader application of this isotope system for stratigraphy and correlation is the lack of reliable, high-resolution, globally representative isotope records that could be assigned a numerical age scale. As such records become available the utility of this system could expand considerably.

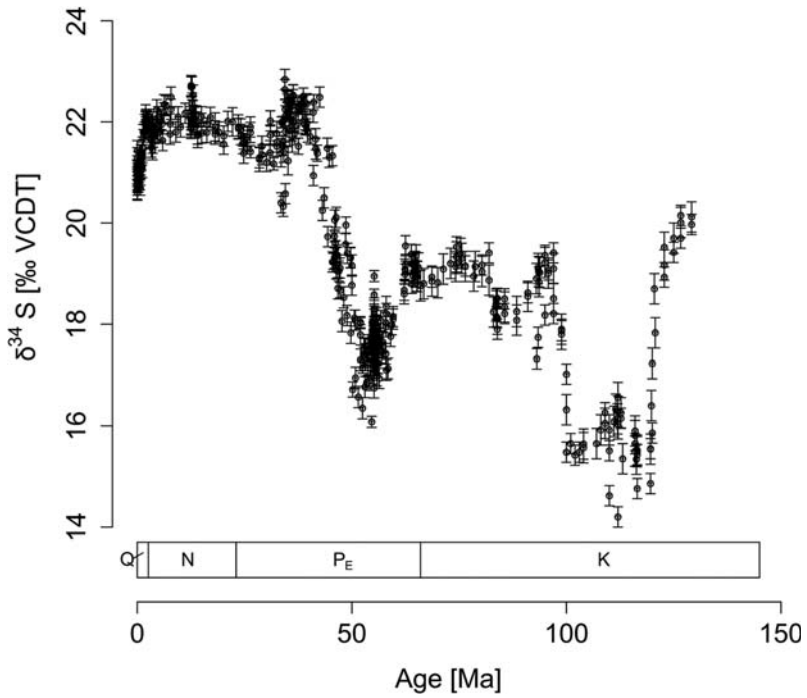

FIGURE 9.2 Seawater sulfate S isotope curve from marine barite for 130 Ma to present. Paytan et al., 1998; Paytan et al., 2004; Turchyn et al., 2009; Markovic et al., 2015; Markovic et al., 2016; Yao et al., 2018; Yao et al., 2020.

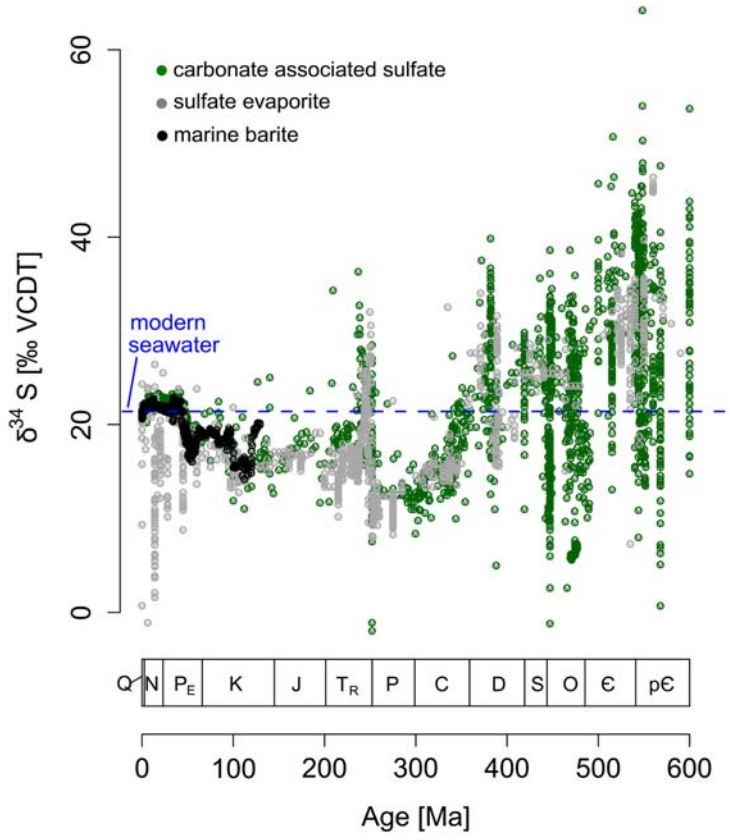

FIGURE 9.3 The Phanerozoic seawater sulfate $\delta^{34}S$ record. Green circles = CAS data (Ueda et al., 1987; Strauss, 1993; Kampschulte and Strauss, 2004; Goldberg et al., 2005; Mazumdar and Strauss, 2006; Gill et al., 2007; Hurtgen et al., 2009; Turchyn et al., 2009; Wu et al., 2010, 2014; Thompson and Kah, 2012; Wotte et al., 2012; Present et al., 2015; Sim et al., 2015; Kah et al., 2016; Schobben et al., 2017; Rennie et al., 2018); gray circles = evaporites data (Holser and Kaplan, 1966; Sakai, 1972; Claypool et al., 1980; Cortecci et al., 1981; Pierre and Rouchy, 1986; Das et al., 1990; Rick, 1990; Utrilla et al., 1992; Fox and Videtich, 1997; Strauss, 1997; Worden et al., 1997; Kampschulte et al., 1998; Strauss, 1993; Strauss et al., 2001; Longinelli and Flora, 2007; Orti et al., 2010; Peryt et al., 2005; Surakotra et al., 2018; Crockford et al., 2019); blue dash line = the modern seawater sulfate $\delta^{34}S$ value of ~21‰. *CAS*, Carbonate-associated sulfate.

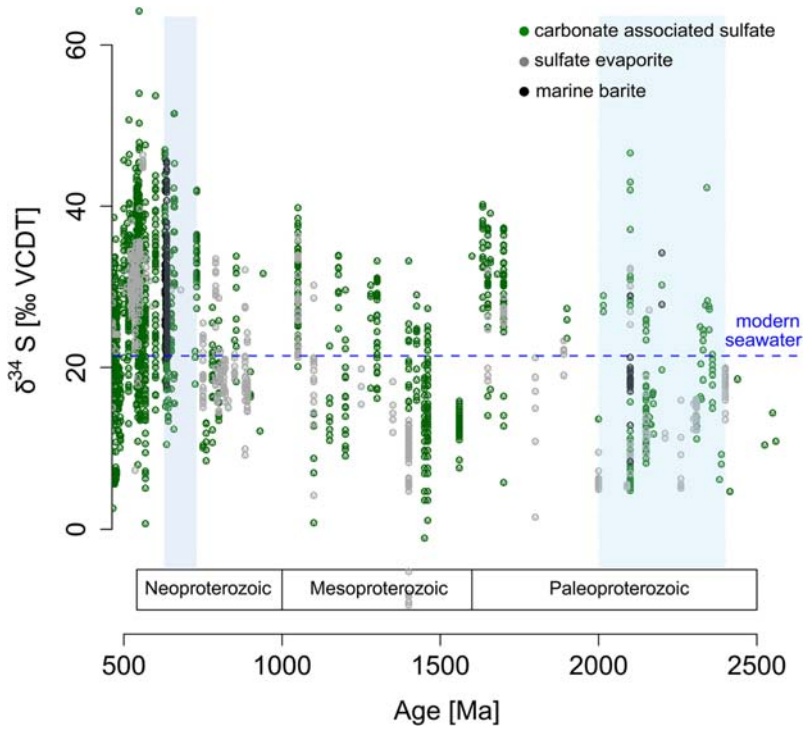

FIGURE 9.4 The Proterozoic seawater sulfate $\delta^{34}S$ curve. Green circles = CAS data; gray circles = evaporites data; Black circles = barite data (Crockford et al., 2019 and references therein). Blue dash line = the modern seawater sulfate $\delta^{34}S$ value of ~21‰. The blue and purple boxes denote the periods of the Great Oxygenation Event (2450–2000 Ma) and Cryogenian (635–717 Ma), respectively. *CAS*, Carbonate-associated sulfate.

9.2 Mechanisms driving the variation in the S isotope record

The chemical and isotopic composition of the ocean changes over time in response to fluctuations in global weathering rates and riverine loads, volcanic activity, hydrothermal exchange rates, sediment diagenesis, and sedimentation and subduction processes. All of these are ultimately controlled by tectonic and climatic changes. Specifically, the oceanic sulfate $\delta^{34}S$ at any given time is controlled by the relative proportion of sulfide and sulfate input and removal from the oceans and their isotopic compositions (e.g., Bottrell and Newton, 2006). S is commonly present in seawater and marine sediments in one of two redox states:

1. in its oxidized state as sulfate and sulfate minerals and
2. in its reduced form as H_2S and sulfide minerals.

The oceanic sulfate $\delta^{34}S$ record provides an estimate for the relative partitioning of S between the oxidized and reduced reservoirs through time. Changes in both input and output of sulfur to/from the ocean have occurred in response to changes in the geological, geochemical, and biological processes (Strauss, 1997; Berner, 1999). These changes are recorded in contemporaneous authigenic minerals that precipitate in the oceanic water column.

Seawater contains a large amount of S ($\sim 40 \times 10^{18}$ mol) that is present, as it has been for at least the past 500 million years, predominantly as oxidized, dissolved sulfate (SO_4^{2-}) (Holser et al., 1988; Berner and Canfield, 1989, 1999). Ancient oceans may have at times had lower sulfate concentrations and thus sulfate residence times may have been shorter (Lowenstein et al., 2001; Horita et al., 2002). The largest input today is from river runoff from the continent. The $\delta^{34}S$ value of this source is variable (0‰–10‰) but typically lower than seawater and depends on the relative amount of gypsum and pyrite in the drainage basin (Krouse, 1980; Arthur, 2000). Volcanism and hydrothermal activity also are small sources of S for the ocean, with $\delta^{34}S$ close to 0‰ (Arthur, 2000). The output flux is via deposition of evaporites and other sulfate-containing minerals ($\delta^{34}S_{evaporite} \approx \delta^{34}S_{seawater}$) and sulfides with $\delta^{34}S$ pyrite ≈ 15‰ (Krouse, 1980; Kaplan, 1983). The typically light isotope ratios of sulfides are a result of the strong S isotope fractionation involved in bacterial sulfate reduction, the precursor for sulfide mineral formation (Krouse, 1980; Kaplan, 1983). This results in the S isotope ratios of seawater sulfate being higher than any of the input sources to the ocean. Seawater sulfate today has a constant $\delta^{34}S$ value of 21.0‰ ± 0.2‰ (Rees et al., 1978). It has also been suggested that in addition to changes in the relative rate of burial of reduced and oxidized S, the marine $\delta^{34}S$ record has been sensitive to the development of a significant reservoir of H_2S in ancient stratified oceans (Newton et al., 2004). Specifically, extreme changes over very short geologic time scales (such as at the Permian–Triassic boundary or the PETM) along with evidence for ocean anoxia could only be explained via the development of a large, relatively short-lived, reservoir of H_2S in the deep

oceanic water column followed by oceanic overturning and reoxygenation of the H_2S (Newton et al., 2004; Algeo et al., 2007; Luo et al., 2010; Yao et al., 2018).

The evidence that the S isotopic composition of seawater sulfate has fluctuated considerably over time, until recently, was based on comprehensive, though not continuous, isotope data sets obtained from marine evaporitic sulfate deposits and pyrite (Claypool et al., 1980; Strauss, 1993). More recently, marine barite has been used to construct a continuous, high-resolution *S* curve for the last 130 Ma (Paytan et al., 1998, 2004; Turchyn et al., 2009; Markovic et al., 2015, 2016; Yao et al., 2018, 2020). Methods to analyze the sulfate that is associated with marine carbonate deposits (carbonate-associated sulfate, CAS) have also been developed, and new data sets using these methods are becoming available. Specifically, CAS has been used to reconstruct global change in the sulfur cycle on both long (Kampschulte and Strauss, 2004) and short (Ohkouchi et al., 1999; Kampschulte et al., 2001) time scales. Particularly, CAS data from Foraminifera that is species-adjusted for fractionation offsets can yield high-quality data (Rennie et al., 2018). The new data from barite and from CAS show considerably more detail and fill significant gaps in the former data sets, revealing previously unrecognized structure and increasing the potential for seawater S isotope curves to serve as a tool for stratigraphy and correlation.

9.3 Isotopic fractionation of sulfur

The sulfur isotope fractionation between evaporitic sulfate minerals and dissolved sulfate is approximately 1‰−2‰ (Thode and Monster, 1965). Experiments and analyses of modern evaporites show values 1.1‰ ± 0.9‰ heavier than dissolved ocean sulfate (Holser and Kaplan, 1966). Modern barites measured by the SF_6 method averaged 0.2‰ heavier than dissolved ocean sulfate (Paytan et al., 1998). Carbonates are also expected to have minor fractionation associated with the incorporation of sulfate. The similarity between the $\delta^{34}S$ value of sulfate minerals and dissolved sulfate means that ancient sulfates can be used as a proxy for the $\delta^{34}S$ value of the ocean at the time that the minerals formed.

Reduced S compounds are mostly produced in association with processes of bacterial sulfate reduction. Dissimilatory reduction (converting sulfate to sulfide) is performed by heterotrophic organisms, particularly sulfate-reducing bacteria. Bacterial sulfate reduction is an energy-yielding, anaerobic process that occurs only in reducing environments (Goldhaber and Kaplan, 1974; Canfield, 2001). Measured fractionations associated with sulfate reduction under experimental conditions range from −20‰ to −46‰ at low rates of sulfate reduction to −10‰ at high reduction rates. The $\delta^{34}S$ values of sulfides of modern marine sediments are typically around −40‰; however, a wide range from −40‰ to +3‰ is observed. Sulfate reduction and iron sulfide precipitation continues only as long as:

1. sulfate is available as an oxidant,
2. organic matter is available for sulfate-reducing bacteria, and
3. reactive iron is present to react with H_2S.

In the marine environment, neither sulfate nor iron generally limits the reaction. Instead, it is the abundance of easily metabolized carbon that controls the extent of sulfate reduction. The broad range of $\delta^{34}S$ values observed in sulfides from marine sediments results from variable fractionation associated with the different sedimentary settings and environmental conditions during sulfate reduction (temperature, porosity, diffusion rates, etc.) as well as other processes in the S cycle that involve fractionation such as sulfur disproportionation reactions (Canfield and Thamdrup, 1994; Habicht et al., 1998).

Assimilatory reduction occurs in autotrophic organisms where sulfur is incorporated in proteins, particularly as S_2^- in amino acids. Assimilatory reduction involves a valence change from +6 to −2. The bonding of the product sulfur is similar to the dissolved sulfate ion, and fractionations are small (+0.5‰ to −4.5‰, Kaplan, 1983). The $\delta^{34}S$ value of organic sulfur in extant marine organisms incorporated by assimilatory processes is generally depleted by 0‰ to 5‰ relative to the ocean.

The wide array of environmental conditions that affect the fractionation, together with the broad range of S isotopic values of sulfide minerals at any given time, and post-depositional alteration of assimilatory S into organic matter, limits the utility of sulfites and S in old organic matter as tools for stratigraphy and correlation, since measured values may not be representative of a global oceanic signature.

9.4 Measurement and materials for sulfur isotope stratigraphy

9.4.1 Isotope analyses

There are four stable isotopes of sulfur. The isotopes that are commonly measured are ^{34}S and ^{32}S, as these are the two most abundant of the four. In most but not all samples, the sulfur isotopes are present in constant ratios to each other, thus the others could be easily computed (but see Farquhar et al., 2000). All values are reported as $\delta^{34}S$ relative to the Canõn Diablo Troilite (CDT) standard (Ault and Jensen, 1963) using the accepted delta notation. Due to scarcity of the CDT standard, secondary synthetic argentite (Ag_2S) and other sulfur-bearing standards have been developed, with $\delta^{34}S$ values being defined relative to

the accepted CTD value of 0‰. Samples are converted to gas (SO_2 or SF_6) and analyzed on a gas-ratio mass spectrometer. Analytical reproducibility is typically ± 0.2‰.

9.4.2 Materials for S isotope analysis

9.4.2.1 Evaporites

Records of oceanic sulfur isotopes through time were originally reconstructed from the analyses of marine evaporitic sulfate minerals (Holser and Kaplan, 1966; Claypool et al., 1980). Evaporites contain abundant sulfate and their formation involves minimal and predictable fractionation, thus they are suitable archives for this analysis. Claypool et al. (1980) presented the first compilation of the secular sulfur isotope record of seawater for the Phanerozoic (Fig. 9.1) and their work provides the basis for our understanding of the sulfur isotope record. However, as a result of the sporadic nature of evaporite formation through geologic time this record is not continuous. Moreover, evaporites are hard to date precisely due to the limited fossil record within these sequences; thus the stratigraphic age control on the evaporitic-based sulfur isotope record is compromised.

9.4.2.2 Barite

Like evaporites, the $\delta^{34}S$ of barite is quite similar to that of sulfate in the solution from which it precipitated. Marine barite precipitates in the oceanic water column and is relatively immune to diagenetic alteration after burial thus it records the changes in the sulfur isotopic composition of seawater through time (Paytan et al., 1998, 2004; Turchyn et al., 2009; Markovic et al., 2015, 2016; Yao et al., 2018, 2020). Moreover, high-resolution, well-dated, and continuous records can be developed as long as barite-containing pelagic marine sediments are available (Paytan et al., 1993). It must be stressed that reliable seawater sulfur isotope records can only be derived from marine (pelagic) barite and not diagenetic or hydrothermal barite deposits (see Eagle et al., 2003 for more details). A sulfur isotope curve was obtained from pelagic marine barites of Cretaceous and Cenozoic ages with unprecedented temporal resolution (Paytan et al., 1998, 2004; Fig. 9.2). The high-resolution curve shows some very rapid changes that could be instrumental for stratigraphic applications.

9.4.2.3 Substituted sulfate in carbonates

Sulfur is a ubiquitous trace element in sedimentary carbonates (e.g., CAS). Concentrations range from several tens of ppm in inorganic carbonates to several thousand ppm in some biogenic carbonates (Burdett et al., 1989; Kampschulte et al., 2001; Lyons et al., 2004). While the mechanism of sulfate incorporation into carbonates is not fully understood, CAS is incorporated with little fractionation thus recording seawater ratios. Carbonates offer an attractive method for refining the secular sulfur curve because of their abundance in the geological record, ease of dating, and relatively high accumulation rates. Indeed, a record for Phanerozoic seawater sulfur isotopes based on CAS has been compiled and published (Kampschulte and Strauss, 2004; Fig. 9.3). Extreme caution must, however, be exercised in extracting CAS from samples and interpreting the sulfur isotope data obtained because carbonates are highly susceptible to postdepositional alteration and secondary mineral precipitation that can obliterate the record. The degree of modification can be assessed by obtaining multiple records from distinct locations (or mineral phases) for the same time interval and construction of secular trends (Kampschulte and Strauss, 2004). Recent work largely overcame these disadvantages by using CAS from single shells of different species of Foraminifera and correcting the data for offsets between species (Rennie et al., 2018).

9.5 A Geologic time scale database

9.5.1 General trends

The current sulfur isotope records include data sets from the Proterozoic to the present (Figs. 9.3–9.5). While the focus of most studies is on shorter time scales and the methods that are used are varied, the overlap among published records and a few long-term studies serve to give a comprehensive view of the sulfur isotope record for the Phanerozoic. Three long-term records have been compiled, two based on evaporites (Claypool et al., 1980; Strauss, 1997) and one based on CAS (Kampschulte and Strauss, 2004). A compilation of data for the Proterozoic was also published (Crockford et al., 2019). Sulfate concentrations in the Proterozoic ocean, however, were much lower than during the Phanerozoic (e.g., Habicht et al., 2002; Kah et al., 2004; Canfield and Farquhar, 2009); hence, it is likely that the oceanic water column was not homogenous with respect to sulfur isotopes limiting the applicability of S isotopes for stratigraphy and correlation.

General trends can be seen in these records. The Proterozoic data show widespread with positive excursions across the Great Oxidation Event and the lower Neoproterozoic. In the Cambrian the average $\delta^{34}S$ value is 34.8 ± 2.8‰ in the CAS record (Kampschulte and Strauss, 2004) and around 30‰ in the evaporite record (Claypool, et al., 1980; Strauss, 1997). These relatively high values are sustained through the Cambrian in the CAS record, ending with anomalously high $\delta^{34}S$ values at the Cambrian/Ordovician boundary. After this point the $\delta^{34}S$ decreases steadily through the remainder of the Paleozoic, reaching a minimum at the Permian/Triassic boundary with an average

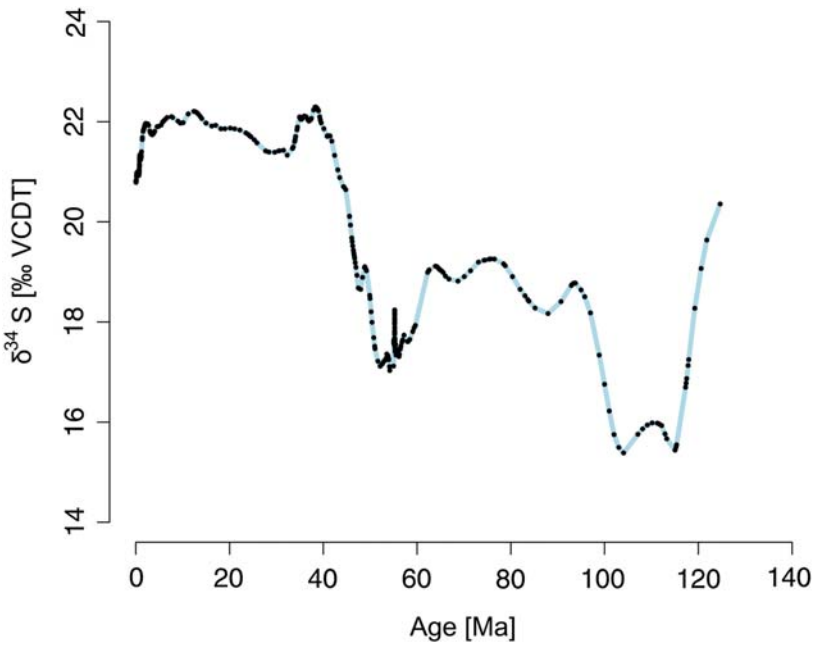

FIGURE 9.5 LOWESS curve for the last 130 million years generated from marine barite data (Paytan et al., 1998, 2004; Turchyn et al., 2009; Markovic et al., 2015, 2016; Yao et al., 2018, 2020); see also Table 9.1.

value of 13.2 ± 2.5‰. A similar but less time-constrained decrease is seen in the evaporite record.

Through the Mesozoic, the $\delta^{34}S$ values are generally lower than in the Paleozoic, ranging between 14‰ and 20‰. The $\delta^{34}S$ values increase quite rapidly from 13.2 ± 2.5‰ at the Permian/Triassic boundary to 17‰ in the Jurassic and decrease again to about 15‰ in the early Cretaceous (Claypool et al., 1980; Strauss, 1997; Kampschulte and Strauss, 2004). The value at the Cretaceous is about 19‰ but two distinct excursions toward lower values are seen: one at ~120 Ma and the other at ~90 Ma (Paytan et al., 2004). A decrease in $\delta^{34}S$ values from ~20‰ to 16‰ is seen in the Paleocene before climbing sharply in the Early to Middle Eocene to the near modern value of 21‰ where it remains steady for the remainder of the Cenozoic (Fig. 9.2).

These broad trends can be useful in obtaining very general stratigraphic information (e.g., typically only at the epoch scale) but are not applicable for age assignments at resolution better than tens of millions of years.

9.5.2 Time boundaries

Strauss (1997) reviewed secular variations in $\delta^{34}S$ across time boundaries characterized by profound biological or geological changes. Due to the paucity of evaporite data, all these time boundary studies have used data obtained from sedimentary sulfides. The premise behind the study of S isotope excursions at age boundaries is based on the expected perturbations in the biosphere which may impact sulfate reduction rates. During a catastrophic event, where productivity plunges, the $\delta^{34}S$ values of the oceans are expected to decrease because of a reduction in organic matter availability, leading to lower sulfate reduction. The subsequent biological radiations should have the opposite effect. Accordingly, the $\delta^{34}S$ values of the oceans should first decrease across a time boundary associated with a catastrophic extinction or major ecosystem reorganization and then increase during the period of recovery. The magnitude of the effect is related to the intensity of the extinction event, the rate of recovery, and the size of the oceanic sulfur reservoir.

Four extinction events have been studied (see Strauss, 1997 for references): the Precambrian–Cambrian, the Frasnian–Famennian, the Permian–Triassic, and the Cretaceous–Tertiary boundaries. Of these, only the Permian–Triassic event shows the expected sulfur trend (Luo et al., 2010). Fluctuations occur at the other boundaries, but no secular (globally concurrent) variations have been observed (see also Newton et al., 2004). In part the reason for the inconsistent results between sections and between extinction events may be related to the inherent problems of analyzing sulfides instead of sulfates and the multitude of controls impacting the isotopic composition of sulfides. Therefore local effects may mask any global sulfur variations. More recent data using CAS Sim et al. (2015) correlated the S isotope record among sections throughout the world representing the Frasnian–Famennian boundary of the Devonian.

9.5.3 Age resolution

Age resolution of the S isotope curve varies with the type of data comprising the record and the specific objectives

for the various studies producing the data. The older sections compiled from evaporite and CAS data have a lower resolution because of the scarcity of evaporites and because CAS depends on the integrity of the carbonates and fossils used for reconstruction, which in many locations, are subjected to extensive postdepositional alteration. In addition, large temporal gaps between samples make it difficult to correlate between sites and thus make exact age determinations challenging. Despite these limitations robust records exist for specific time periods and the confidence within each such time interval is considerably improved from the earlier evaporate records. Age resolution of records based on barite is much better but so far barite has been recovered predominantly from pelagic sediments, limiting the applicability to the last 130 Ma.

The Phanerozoic evaporite record, compiled by Claypool et al. (1980) with further work done by Strauss (1997), has several characteristics that make it difficult to use for S stratigraphy. First, the record has large gaps in it that leave long periods of time unaccounted for. In Claypool et al. (1980) a best estimate curve was visually approximated to combine and extrapolate between disparate data sets; however, this eliminates the ability to detect finer fluctuations that may be present. Second, the absolute S isotope values recorded at each time point range considerably, confounding the issue. The range of $\delta^{34}S$ values within each time interval is approximately 5‰ for most of the data sets, which makes pinpointing an age from a stratigraphic perspective difficult since in many cases the broad fluctuations that occur over time are within ±5‰ (Fig. 9.1). Third, the ages used for each sample are approximate due to the scarcity of fossils in sections used to compile the isotope curves. Even in the evaporite record from Strauss (1993) that derives its ages after Harland et al. (1990), the age uncertainty spans more than 10 million years depending on the segment (or specific time range), which makes it difficult to use these data for stratigraphic correlation (Strauss, 1993).

The S isotope record derived from CAS is more robust (Fig. 9.3). The record is consistent with the evaporite data in the broad strokes (Fig. 9.4) but a better constraint on the ages of the samples is possible. The data set presented in Kampschulte and Strauss (2004) and references therein show a record for the Phanerozoic that reduces the uncertainty in age and S isotope values considerably from those associated with evaporites. The CAS samples were taken from stratigraphically well-constrained biogenic calcites (using the time scale of Harland et al., 1990) with a resolution of 1−5 million years within data sets. However, the data sets analyzed are not continuous, leaving gaps, that while not as glaring as those in the evaporite record, still limit the accuracy of a smooth curve and may miss finer details. The CAS data that represent older ages have a wider range of S isotope values than that of more recent (younger) samples. For example, a "scatter" of ±10‰ and even up to 20‰ in the Cambrian and Ordovician for samples with similar ages. More recent samples have narrower ranges, from 5‰ to 10‰, and thus would be more useful for stratigraphy, although in some places, the low temporal resolution still makes it difficult to distinguish noise from trend (Kampschulte and Strauss, 2004).

The data compiled and presented in Kampschulte and Strauss (2004) use a moving average to create a continuous curve (Fig. 9.4). The effect is to smooth out the observed variation that then makes it difficult to assess the error associated with both the isotope data set (e.g., $\delta^{34}S$) and the age resolution. This makes it difficult to resolve trends and compare the data with other records or to use the curve for precise sample age determination. The smoothed curve of Kampschulte and Strauss (2004) can, however, be used to assess the utility of certain sections (age intervals) of the record for dating using S stratigraphy, but because the specific data sets used to produce the smooth curve were not available to us, evaluation of age resolution or a detailed statistical LOWESS fit (McArthur et al., 2001) for derivation of numeric ages using the CAS record cannot be compiled at this time. The analysis of $\delta^{34}S$ hosted in the calcite lattice of single-species foraminifera vastly improved stratigraphy afforded by CAS-based records although corrections for species-specific fractionation must be applied (Rennie et al., 2018). The published Cenozoic foraminifera record agrees well with the barite-derived record (Yao et al., 2020).

The marine barite record presented by Paytan et al. (1998, 2004) is derived from ocean floor sediment. The current record goes back ~130 Ma. The barite-based S isotope curve provides a record with a resolution of less than 1 million years with very few gaps. The age of the samples is constrained by biostratigraphy and Sr isotopes and typically has an error of less than 100,000 years. The continuous and secular (based on data from multiple sites for each time interval) nature and the high resolution of this record illuminate finer features that are missed in the lower resolution evaporite and CAS records. The record also has a narrower range of S isotope values for each time point, further constraining the curve. These features make it the most robust of the three available records thus far and the most useful for stratigraphy, for the periods it covers. This record serves to illustrate the potential use of S isotopes for stratigraphy and as more such detailed high-resolution secular records (e.g., based on coherent data from multiple locations and settings) become available for different geological periods, S isotope stratigraphy can be more widely utilized. At the moment the limited availability of continuous high-resolution secular data and the need for updated and better constrained ages for previously published records are the biggest obstacles to using sulfur isotopes as a stratigraphic tool.

9.5.4 Specific age intervals

While the current S record of the Phanerozoic is not ideal for stratigraphic applications as discussed previously, there is still potential for using S as a stratigraphic tool for certain time intervals. The time periods best suited to dating are those that are distinguished by rapid changes in $\delta^{34}S$. Identifying smaller fluctuations on the "plateaus" of the isotope curve is difficult because of the limited temporal resolution, and the relatively large error in the $\delta^{34}S$ compared to the small fluctuations. These limitations make the potential use of fine features for stratigraphic and correlation purposes impossible at this stage.

At this time the most useful record for S stratigraphy applications is the marine barite curve that extends back to 130 Ma. The distinct features that appear in this high-resolution curve show five time periods with relatively abrupt changes in $\delta^{34}S$ that could lead to precise dating: 130–116, 107–96, 96–86, 83–75, 65–40, and ~2 Ma to the present. Resolving ages during periods of smaller fluctuations is possible but would likely necessitate a much larger data set in order to match multiple points and avoid offsets between data from distinct sites. The plateaus, notably from ~30 Ma to about 2 Ma where the S isotope values do not significantly change, are not useful because there are few features that can be teased out and distinguished from sampling and analytical error.

Next we present the trends in the $\delta^{34}S$ isotope data for each time period and a brief discussion of the utility of the data for stratigraphy is presented. Kampschulte and Strauss (2004) showed that the Phanerozoic CAS record is consistent with and better constrained temporally than the evaporite record. For this reason the trends discussed next will rely on the CAS record from the Cambrian to the Jurassic (Kampschulte and Strauss, 2004, and references therein) and the barite record from Paytan et al., 1998, 2004; Turchyn et al., 2009; Markovic et al., 2015, 2016; and Yao et al., 2018, 2020, from the Cretaceous to the present, unless otherwise specified. Recent studies also showed that multiple sulfur isotopes (^{33}S and ^{36}S) of sulfate in the Proterozoic could be powerful tools for stratigraphy (e.g., Crockford et al., 2019; Farquhar and Wing, 2003; Johnston, 2011 and references therein). However, the use of ^{33}S and ^{36}S has so far been limited and will not be further discussed here.

9.5.4.1 Cambrian

The seawater $\delta^{34}S$ records for the Cambrian are derived from carbonate and evaporite rocks (and a few from barite) in Australia, Canada, China, India, Russia, Spain, and France (Goldberg et al., 2005; Hough et al., 2006; Hurtgen et al., 2009; Mazumdar and Strauss, 2006; Peryt et al., 2005; Wotte et al., 2012). The values recorded represent a wide range. The data show an excursion with a maximum of 50‰ in the lower Cambrian, followed by a systematic >15‰ decrease across the middle–upper Cambrian. The mean value is relatively high (>30‰), although it is unclear if these high values reflect open ocean seawater sulfate or if the integrity of these samples was compromised. The high values and intrabasin variability may partially result from the intrabasin microbial sulfate reduction under sulfate limitation or diagenetic processes as well as euxinic conditions (Goldberg et al., 2005; Mazumdar and Strauss, 2006; Peryt et al., 2005; Hough et al., 2006).

The age resolution that can be theoretically obtained using the moving mean curve is 2.0 Myr from 535 to 525 Ma and 2.8 Myr from 525 to 511 Ma (but note that the curve averages values over 5 Myr) (Kampschulte and Strauss, 2004). When looking at the raw data, one sees that there is a significant age gap between the two time periods sampled that is smoothed over in the moving mean. In addition, while the $\delta^{34}S$ values in both data sets are relatively high (>30‰) and can be used to identify samples of Cambrian age, the range of values is similar for both sets and thus without a larger data set that fills in the gaps, distinguishing between older and younger samples within the Cambrian may be difficult. The global nature of the record should also be verified as sulfate was most likely a nonconservative anion in the Cambrian ocean (Wotte et al., 2012).

9.5.4.2 Ordovician

The CAS record in the Ordovician is composed of 16 samples. The temporal resolution of the record is between 1 and 8 Myr with the older samples dominantly ~4 million years apart and the younger samples 1 million years apart. The $\delta^{34}S$ values were determined from whole rock in 15 of these samples, and for 12 of them brachiopod shells were also used. The record shows a decrease from a moving mean of 30‰ in the Lower Ordovician to 24‰ in the uppermost Ordovician (Kampschulte and Strauss, 2004).

The wide range of the measured $\delta^{34}S$ values (15‰–30‰) throughout the period complicates the picture. Without a higher resolution data set it is impossible to distinguish whether the broad range represents real fluctuations and the lower values (15‰) are a true minimum. Specifically, when considering the time resolution of the record, values of 15‰ and ~30‰ that occur within the same time frame render the use of such records unreliable. However, on a broader scale, the moving average of $\delta^{34}S$ values, which plateaus around 24‰ at ~475 Ma and remain at that level up to the Ordovician/Silurian boundary, can be distinguished from other time periods.

9.5.4.3 Silurian

The Silurian shows a continued trend of decreasing $\delta^{34}S$ values with a range from 35.6‰ to 21.5‰ in the CAS

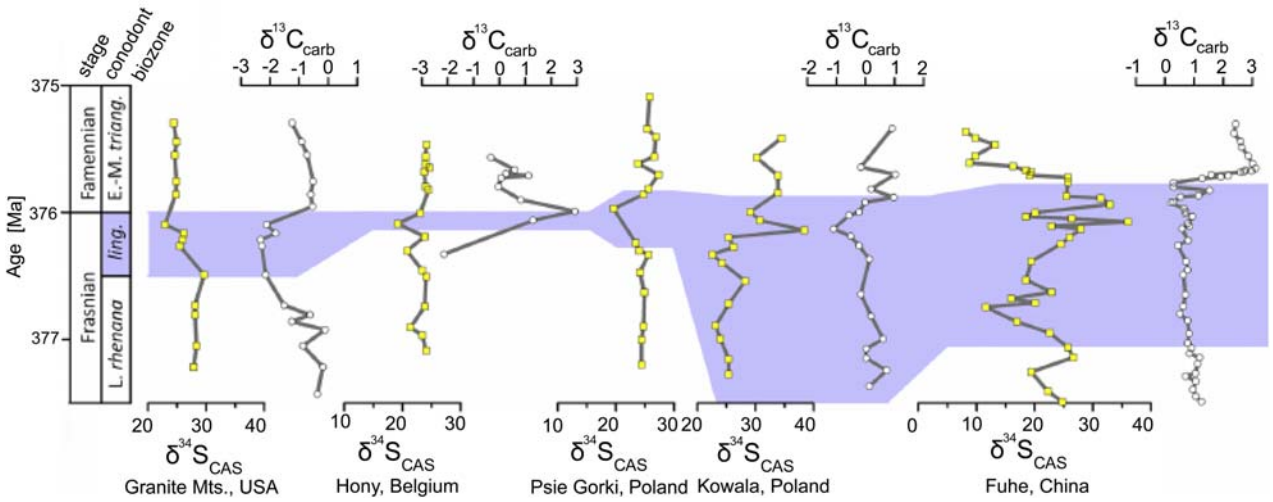

FIGURE 9.6 Sulfur and carbon isotope records across the Frasnian–Famennian boundary. There is a brief $\delta^{34}S$ drop throughout the linguiformis biozone and a positive $\delta^{13}C$ excursion starting in the uppermost part of this biozone. The shaded area denotes the linguiformis conodont biozone. Abbreviations: *L. rhenana*, Late *rhenana*; *ling.*, *linguiformis* E.–M. *triang.*, Early to middle triangularis. Figure after Sim et al. (2015).

record in 15 brachiopod shells and 17 whole rock samples over 30 Myr (Kampschulte and Strauss, 2004). The Ordovician/Silurian boundary exhibits the higher values (30‰–35, which drop by 1‰–2‰ in the Early Silurian. Following is a narrower range of S isotope values from ~24‰ to 28‰ and the moving mean shows a plateau in the record. The running mean seems to smooth away the slight downward trend seen in the raw data. Having the mean at odds with the trend in the raw data makes utility of the curve from this section within the Silurian difficult to use for stratigraphic dating because there is no good method to resolve the inconsistencies without a more complete record. Nevertheless, the range from ~24‰ to 28‰ is distinctive to the Late Ordovician and Silurian.

9.5.4.4 Devonian

A total of 18 samples comprise the record for the Devonian. $\delta^{34}S$ values in the Devonian show a downward trend, decreasing from ~25‰ in the Late Silurian to ~19‰ in the lower Middle Devonian. The steep slope of the curve from 408 to 395 Ma makes it useful for stratigraphy, specifically a 6‰ change over 13 million years and an isotope analytical error of 0.2‰ can yield an age resolution in the range of 0.5 million years. In the second section, from 395 to 381 Ma, the curve plateaus: the moving average remains around 18.8–19.2. The remainder of the Devonian exhibits a distinctive peak with $\delta^{34}S$ increasing from 23‰ in the Frasnian age of the Late Devonian (371 Ma) to a maximum of 26.9‰ (Kampschulte and Strauss, 2004). The age resolution of the data set varies from 1 to 4 Myr with a gap of 8 million years over the Devonian/Carboniferous boundary. The shape of the curve makes this section distinct and thus potentially useful for stratigraphy; however, the moving mean currently smooths the data. It is noteworthy that Sim et al. (2015) correlated the S isotope record among sections throughout the world representing the Frasnian–Famennian boundary, despite relatively low-resolution data available at that time. The generally similar ~5‰ decline in seawater $\delta^{34}S$ has been reported for sections in the United States, Belgium, and Poland, which has the potential for correlation applications as seen in Fig. 9.6 (Sim et al., 2015 and references therein). Moreover, the $\delta^{34}S$ and $\delta^{13}C$ excursions may be linked to the Late Devonian mass extinction (Sim et al., 2015). It is, however, important to obtain more data with better defined ages from diverse sites to verify a global trend.

9.5.4.5 Carboniferous

The Carboniferous is also characterized by a decrease in the CAS data from ~20‰ in the Early Carboniferous (Mississippian) to ~15‰ at 334 Ma where it remains until decreasing to around 12‰ in the Late Carboniferous (Pennsylvanian: Kampschulte et al., 2001; Kampschulte and Strauss, 2004; Surakotra et al., 2018). The age resolution of the record, based on the moving mean, ranges from 5.6 Myr from 362 to 334 Ma in the Mississippian and 3–4 Myr for the remainder of the period. The overall range of values in the raw data is narrower than for other section, which makes distinguishing between noise and trend easier. However, the values plateau from 342.8 to 309.2 Ma and leave only the beginning and end of the period significantly distinguishable for stratigraphic correlation. Thus there is a potential for stratigraphic applications for the Early and Late Carboniferous provided the available data are indeed

representative of global trends. The potential age resolution for these time intervals is in the range of about 1 million years (5‰ change over about 20 Myr).

9.5.4.6 Permian

The Permian record maintains the low $\delta^{34}S$ values that characterize the end of the Carboniferous, around 12‰. This value is seen in the 16 samples analyzed for the Permian (Kampschulte and Strauss, 2004). This overall $\delta^{34}S$ value is distinctive for the period and is useful for dating the period as a whole but the plateau in the record does not lend itself to more precise stratigraphic dating or correlation within the Permian.

The Permian/Triassic boundary has been sampled at higher resolution of 1 Myr (Kramm and Wedepohl, 1991; Scholle, 1995; Newton et al., 2004; Algeo et al., 2007; Gorjan et al., 2007) and shows distinct fluctuations that are useful stratigraphically (see next).

9.5.4.7 Triassic

The transition from the Paleozoic to the Mesozoic is characterized by an abrupt increase in the seawater $\delta^{34}S$ value from 12‰ in the upper Permian to a maximum value of ~30‰ across the Permian–Triassic boundary (Cortecci et al., 1981; Worden et al., 1997; Kampschulte and Strauss 2004; Newton et al., 2004; Algeo et al., 2007; Longinelli and Flora, 2007; Luo et al., 2010; Song et al., 2014; Schobben et al., 2017; Bernasconi et al., 2017). This peak value occurs at the top of the Permian–Triassic extinction interval followed by a sharp drop to around a mean of 17‰ in the lower and middle Triassic. These data have been sampled from worldwide locations at a temporal resolution of less than 1 million years (Fig. 9.7), indicating that the striking fluctuation is a predominant and global signal. Previous studies interpreted such extreme changes as evidence for the development of a sizable, relatively short-lived reservoir of reduced sulfur in the deep oceanic water column followed by oceanic overturning and sulfide reoxidation (Newton et al., 2004; Algeo et al., 2007; Luo et al., 2010; Bernasconi et al., 2017). The estimated seawater sulfate concentrations were relatively low for the end Permian and the early Triassic, varying between 2 and 6 mM (Bernasconi et al., 2017). More importantly, the positive excursion of more than 10‰ over a time scale of a few million years or even less allows for robust stratigraphic correlations (e.g., Luo et al., 2010). For the remainder of the Triassic the seawater $\delta^{34}S$ value remains relatively constant at approximately 16‰, followed by short-term fluctuations between 11‰ and 25‰ in the uppermost Triassic. The period of distinct variations is potentially suitable for correlations.

9.5.4.8 Jurassic

The $\delta^{34}S$ data for the Jurassic seawater sulfate cluster between 14‰ and 18.0‰ with two maxima of 23.4‰ in the lower Middle Jurassic (Toarcian) and 20.7‰ in the upper Middle Jurassic (Bathonian) (Claypool et al., 1980; Kampschulte and Strauss, 2004; Williford et al., 2009; Gill et al., 2011; Newton et al., 2011). The positive excursion is attributed to the early Toarcian Oceanic Anoxic Event (183 Ma) with the spread of euxinic (i.e., anoxic and sulfidic) bottom waters and thus increases in pyrite burial (Jenkyns, 1988; Williford et al., 2009; Jenkyns, 2010; Gill et al., 2011; Newton et al., 2011). This drastic change coincides with the widespread extinction of benthic organisms in the Northern Europe (Jenkyns, 1988). The temporal resolution of the evaporite and CAS data for the Toarcian and Pliensbachian is constrained on the sub-million-year scale providing more precise information of seawater $\delta^{34}S$ variations, which could be used for stratigraphy. However, for the rest of the Jurassic the overall age uncertainty is relatively large, and more data are required to show finer $\delta^{34}S$ changes.

9.5.4.9 Cretaceous

The Cretaceous record (Fig. 9.2) derived from marine barite by Paytan et al. (2004) and DeBond et al. (2012) is a continuous record that has a resolution of less than 1 million years. A negative shift from ~20‰ to 15‰ occurs from 130 to 120 Ma, remaining low until 104 Ma when it rises to ~19‰ over 10 million years. There is a small minimum at 88 Ma with a value of 18.3‰, returning to values of 18‰–19‰ at ~80 Ma for the remainder of the period.

These results generally agree with the CAS data from Kampschulte and Strauss (2004). This record and the observed fluctuations further illuminate variations that can be seen when the finer scale not smoothed record is available. The finer detail and the observed changes that occur in the beginning of this period make this record useful for stratigraphy and will be discussed later in the chapter. Specifically, both negative excursions (130–120 and 80–87 Ma) occur on relatively short time scales, likely due to the lower seawater sulfate concentration in the Cretaceous (Horita et al., 2002), which allow for correlation and can provide stratigraphic constraints.

9.5.4.10 Cenozoic

A high-resolution barite curve for the Cenozoic (Fig. 9.2) with an age resolution of <1 Myr shows $\delta^{34}S$ values of ~19‰ at the Cretaceous/Paleogene boundary, which drop precipitously to ~17‰ at the Paleocene/Eocene boundary (Paytan et al., 1998; Markovic et al., 2015; Rennie et al., 2018; Yao et al., 2020). Following this minimum, a relatively rapid rise to ~22‰ in the Early to

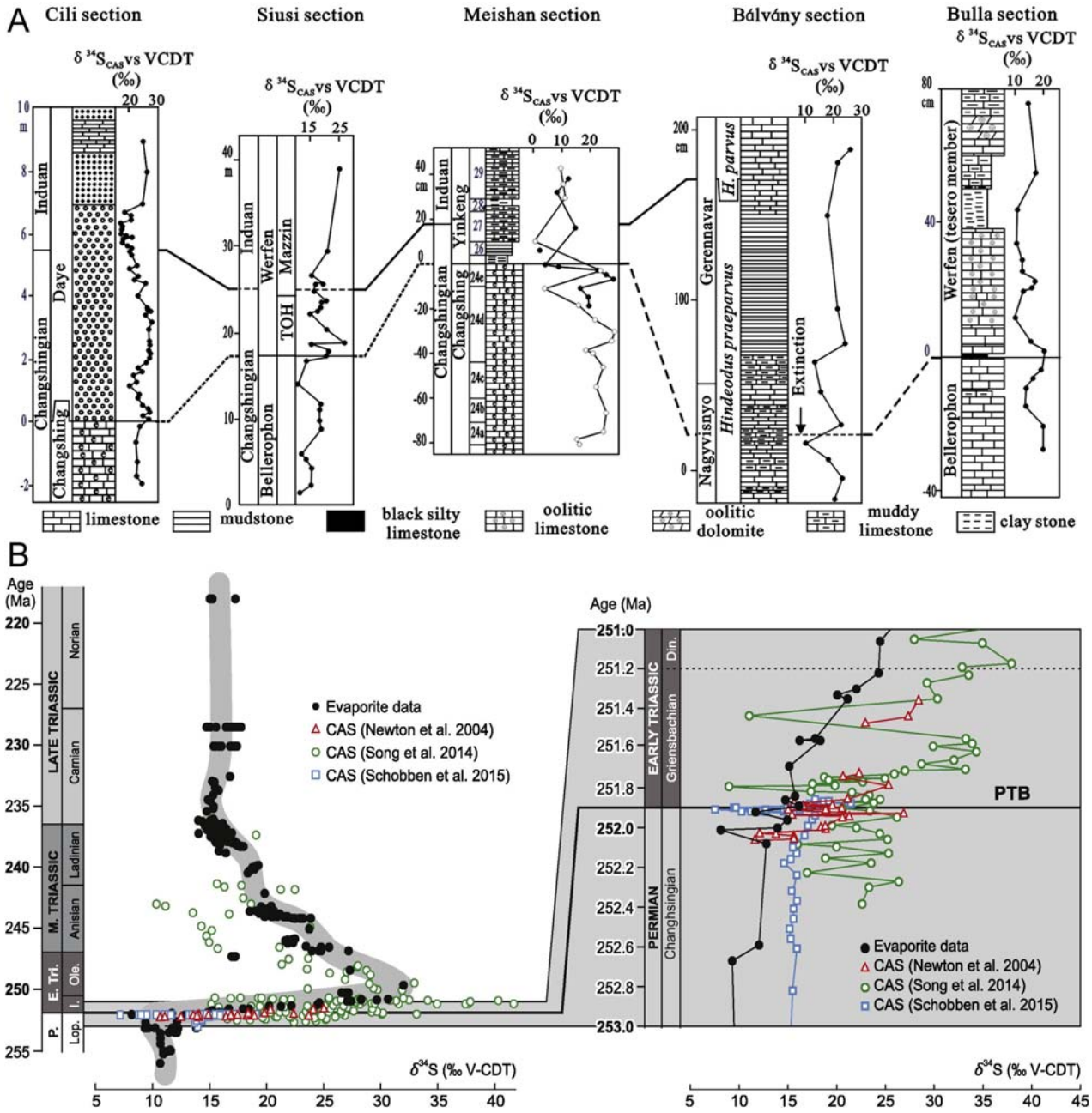

FIGURE 9.7 (A) The CAS-based sulfur isotope records across the Permian–Triassic boundary at different sections from worldwide locations. (B) Comparison of the evaporite-based and CAS-based sulfur isotope records across the Permian–Triassic boundary. *CAS*, Carbonate-associated sulfate. Panel (A): After Luo et al., 2010. Panel (B): After Bernasconi et al., 2017.

Mid-Eocene is observed and this value is maintained until the Pleistocene. The decrease and increase observed between 65 and 40 Ma are useful for stratigraphic purposes (see next). A distinct peak is seen at the PETM (Yao et al., 2018) and a decrease of about 1‰ over the last 2 million years is also evident as reported in Markovic et al. (2015, 2016). In the previous barite record the Eocene rise of seawater $\delta^{34}S$ is defined by only a few samples from Deep Sea Drilling Project Site 366 (Paytan et al., 1998), where the biostratigraphy is not well constrained (Lancelot et al., 1977, 2016). In addition, the decreasing porewater sulfate concentrations with depth, generally higher sedimentation rates (29–41.5 m/Myr), and observable pyrite occurrences at Site 366 throughout the middle to lower Eocene sections (38–56 Ma) imply an organic-rich and reducing environment during this

time (Boersma and Shackleton, 1977; Lancelot et al., 1977; Couture et al., 1977), which suggest that the barite in that section could have been diagenetically altered. Taking advantage of more recently retrieved cores and a much improved biostratigraphic framework, Yao et al. (2020) recently evaluated and refined the Eocene $\delta^{34}S$ data with a new high-resolution barite-based $\delta^{34}S$ record between 60 and 30 Ma. They showed anomalously high $^{87}Sr/^{86}Sr$ ratios of Site 366 barites older than 38 Ma, indicating that the local conditions at Site 366 during the Eocene allowed for sulfate reduction and the formation of diagenetic barite.

9.6 A database of S isotope values and their ages for the past 130 Myr using LOWESS regression

At this early stage of development for S isotope stratigraphy, we can see the general trends for the record throughout the Phanerozoic. These trends and values can be used for broad age assignments and correlations at distinct intervals with defined excursions (e.g., the Permian–Triassic Boundary). The goal of developing a LOWESS regression curve for S isotopes and accompanying lookup tables is not yet realized. Currently, the limits to developing such tables include the availability of raw data to construct secular trends, the unknown error associated with age assignments, and gaps in the data sets. The potential for using LOWESS regression, however, can be illustrated by the marine barite data sets over the Cretaceous and Cenozoic (Fig. 9.5). The LOWESS regression curve shown in Fig. 9.5 was produced according to (McArthur et al., 2001).

Based on the LOWESS curve we calculated the age resolution associated with the five age intervals that exhibit abrupt changes in $\delta^{34}S$, 130–116, 107–96, 96–86, 83–75, 65–40, and ~2 Ma to the present. Age resolutions are 0.5, 0.7, 2.6, 2.1, 1.5, and 0.9 Myr, respectively, based on the data and an analytical error of 0.2‰. From this curve we also generated a preliminary lookup table for the data set (Table 9.1).

9.7 Use of S isotopes for correlation

S isotopes have not been widely used as the sole stratigraphic tool for dating samples. The few samples in the literature of S isotopes used for dating and correlation all also use other methods such as $\delta^{13}C$ and $^{87}Sr/^{86}Sr$ at the same time (Walter et al., 2000; Pokrovskii et al., 2006; Misi et al., 2007). Some studies, particularly those focused on the Permian/Triassic Boundary (Scholle, 1995; Kramm and Wedepohl, 1991; Algeo, et al., 2007; Gorjan et al., 2007), use $\delta^{13}C$, $^{87}Sr/^{86}Sr$, biostratigraphy, paleomagnetism, and other methods to correlate the S isotope records and use the S data to investigate the causes and consequences of various biogeochemical cycles across the boundary. Nevertheless, the secular and defined trend in the S isotope record at this time interval could be used for correlation and age determination in the future where methods other than S isotopes are not available or to refine age assignments based on other records.

The utility of using S isotopes for correlation between sites is illustrated in Fig. 9.8 from Yao et al. (2018). This study focuses on the Paleocene Eocene Thermal Maximum at 56 Ma. Ocean Drilling Program Site 1051 is located in the North Atlantic and does not have as distinct a record of the Carbon Isotope Excursion in the $\delta^{13}C$ record that is typically used for correlation purposes of

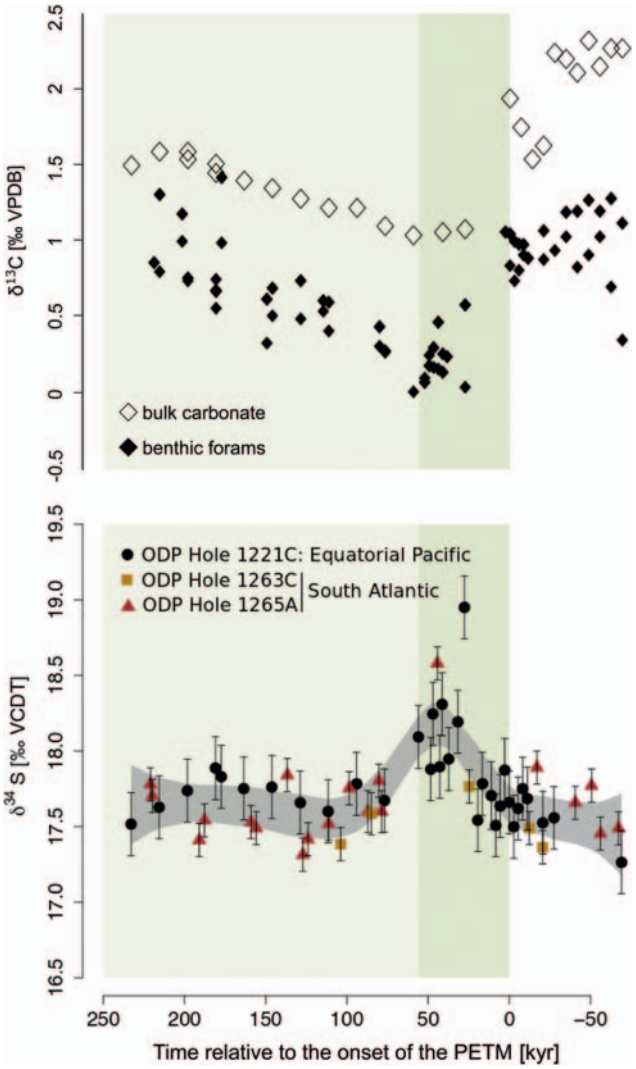

FIGURE 9.8 The sulfur and carbon isotope records across the PETM. Open and solid diamonds denote the $\delta^{13}C$ data derived from bulk carbonate and benthic Foraminifera from ODP Hole 1221A (Nunes and Norris, 2005). Black circles, yellow squares, and red triangles denote the barite-based seawater $\delta^{34}S$ data (1σ) from ODP Hole 1221A, 1263C, and 1265A (Yao et al., 2018). The gray envelope denotes the 95% confidence interval of the LOESS regression for the total $\delta^{34}S$ data. Ages and the PETM stages (*shaded boxes*) as defined by Nunes and Norris (2005).

TABLE 9.1 Preliminary lookup table for the data set of Fig. 9.5.

Age (Ma)	$\delta^{34}S$ Barite	Error (±)
0.00	20.86	0.20
0.00	21.05	0.20
0.02	20.70	0.15
0.03	20.70	0.15
0.05	20.60	0.15
0.07	20.70	0.15
0.08	20.80	0.20
0.08	20.80	0.15
0.12	21.04	0.20
0.16	20.70	0.15
0.17	20.80	0.15
0.18	21.00	0.15
0.19	20.90	0.15
0.20	20.98	0.20
0.24	21.21	0.20
0.24	21.10	0.15
0.30	20.90	0.15
0.31	20.81	0.20
0.38	20.80	0.15
0.39	21.00	0.20
0.40	20.90	0.20
0.42	21.10	0.15
0.48	20.93	0.18
0.53	21.10	0.15
0.61	21.00	0.15
0.61	20.86	0.20
0.62	20.90	0.15
0.66	20.90	0.15
0.66	20.90	0.15
0.68	21.14	0.20
0.69	20.85	0.15
0.69	20.90	0.15
0.71	21.00	0.15
0.72	21.10	0.15
0.74	20.90	0.15
0.76	21.22	0.20

(Continued)

TABLE 9.1 (Continued)

Age (Ma)	$\delta^{34}S$ Barite	Error (±)
0.76	21.08	0.20
0.77	21.10	0.15
0.78	21.10	0.15
0.79	21.20	0.15
0.81	21.30	0.15
0.82	21.30	0.15
0.83	21.30	0.15
0.85	21.40	0.15
0.91	21.34	0.20
0.92	21.30	0.15
0.92	21.20	0.15
0.96	21.20	0.15
0.98	21.20	0.15
1.03	21.35	0.20
1.12	21.30	0.15
1.14	21.10	0.20
1.16	21.40	0.15
1.21	21.45	0.20
1.37	21.80	0.15
1.40	21.70	0.15
1.55	21.80	0.15
1.58	21.80	0.15
1.61	21.80	0.15
1.71	21.80	0.20
1.75	22.00	0.15
1.80	21.80	0.15
1.93	21.80	0.15
1.94	22.05	0.20
1.95	21.90	0.15
2.01	21.90	0.20
2.02	22.10	0.15
2.10	22.00	0.15
2.14	21.90	0.15
2.26	21.90	0.15
2.28	22.02	0.20
2.34	22.00	0.15
2.54	21.80	0.20

(Continued)

TABLE 9.1 (Continued)

Age (Ma)	$\delta^{34}S$ Barite	Error (±)
2.74	22.10	0.15
2.98	21.90	0.15
3.05	21.67	0.20
3.09	21.85	0.20
3.30	21.50	0.20
3.50	21.90	0.20
3.58	21.51	0.20
3.65	21.95	0.20
3.72	21.70	0.20
3.83	21.90	0.20
4.02	21.77	0.20
4.55	22.04	0.20
4.85	21.94	0.20
5.40	21.93	0.20
5.74	21.96	0.20
5.90	21.63	0.20
6.23	22.26	0.20
6.68	22.32	0.20
7.64	21.86	0.20
7.85	22.37	0.20
9.00	21.80	0.20
9.50	22.10	0.20
10.10	21.90	0.20
11.17	22.17	0.20
12.40	22.10	0.20
12.49	21.96	0.20
12.50	21.90	0.20
12.54	22.71	0.20
12.60	21.98	0.24
12.77	22.70	0.20
12.78	22.30	0.20
13.00	22.35	0.22
13.27	22.04	0.20
13.72	22.06	0.20
14.05	21.75	0.22
14.95	22.10	0.20
14.98	21.87	0.20

(Continued)

TABLE 9.1 (Continued)

Age (Ma)	$\delta^{34}S$ Barite	Error (±)
16.20	21.88	0.16
17.04	22.09	0.20
18.13	21.83	0.23
19.00	21.80	0.20
20.14	21.64	0.20
21.08	22.01	0.20
22.20	22.00	0.28
23.47	21.89	0.22
23.97	21.81	0.20
24.36	21.64	0.20
24.52	21.48	0.16
25.26	21.66	0.20
25.83	21.70	0.17
27.68	21.27	0.22
28.38	21.44	0.20
29.61	21.20	0.18
30.50	21.39	0.24
30.60	21.83	0.19
31.48	21.17	0.12
32.30	21.52	0.20
33.44	21.32	0.21
33.49	21.39	0.28
33.58	21.99	0.11
33.90	21.57	0.16
33.92	22.00	0.11
34.00	20.33	0.20
34.10	21.40	0.20
34.39	22.74	0.20
34.44	22.25	0.20
34.49	21.50	0.23
34.93	22.29	0.17
35.02	22.40	0.20
35.10	21.23	0.28
35.17	22.16	0.11
35.37	22.02	0.20
35.49	22.26	0.20
35.76	22.14	0.21

(Continued)

TABLE 9.1 (Continued)

Age (Ma)	$\delta^{34}S$ Barite	Error (±)
35.95	22.05	0.18
35.96	22.39	0.11
36.05	21.60	0.20
36.25	22.52	0.18
36.37	22.03	0.16
36.72	21.78	0.11
36.95	22.17	0.20
37.33	22.31	0.16
37.42	22.14	0.16
37.46	21.52	0.16
37.94	22.36	0.16
38.23	22.32	0.16
38.32	22.20	0.16
38.39	22.36	0.15
38.59	22.51	0.16
38.88	22.00	0.21
38.96	22.37	0.16
39.24	21.91	0.15
39.36	21.98	0.16
39.37	22.36	0.20
39.55	21.80	0.20
40.12	21.71	0.15
40.83	22.19	0.20
40.87	20.94	0.20
40.95	22.39	0.15
41.41	21.66	0.21
41.46	21.47	0.21
41.83	21.38	0.16
42.42	22.49	0.20
43.10	20.25	0.20
43.52	20.50	0.20
44.30	21.48	0.20
44.42	19.73	0.20
44.81	21.30	0.20
45.58	19.23	0.20
45.60	21.33	0.20
45.80	19.24	0.16

(Continued)

TABLE 9.1 (Continued)

Age (Ma)	$\delta^{34}S$ Barite	Error (±)
46.08	19.74	0.11
46.16	19.69	0.20
46.28	19.61	0.20
46.42	19.49	0.16
46.51	19.74	0.18
46.58	19.09	0.20
46.61	19.37	0.20
46.68	19.06	0.16
46.81	19.36	0.16
46.96	18.71	0.21
47.18	19.05	0.20
47.48	19.11	0.20
47.49	18.67	0.15
47.96	18.06	0.21
48.37	18.53	0.21
48.79	19.58	0.21
48.85	19.96	0.16
49.09	18.17	0.20
49.20	19.40	0.20
49.91	19.31	0.20
49.97	17.83	0.21
50.20	18.97	0.21
50.39	16.72	0.15
50.76	18.12	0.16
50.97	18.08	0.20
51.02	16.95	0.21
51.66	16.57	0.21
52.13	17.95	0.14
52.14	17.30	0.21
52.60	16.35	0.21
52.61	17.15	0.11
52.92	17.42	0.17
53.14	16.77	0.21
53.26	17.58	0.15
53.33	17.40	0.21
53.37	17.45	0.11
53.54	16.86	0.11

(Continued)

TABLE 9.1 (Continued)

Age (Ma)	$\delta^{34}S$ Barite	Error (±)
53.78	17.21	0.21
53.90	17.68	0.11
53.96	17.50	0.21
54.13	16.90	0.11
54.19	16.90	0.20
54.67	16.08	0.11
54.98	17.11	0.21
55.03	17.52	0.11
55.05	17.78	0.11
55.05	17.70	0.11
55.05	17.63	0.21
55.07	17.74	0.14
55.07	17.41	0.14
55.08	17.54	0.11
55.08	17.89	0.14
55.09	17.83	0.21
55.09	17.04	0.21
55.10	17.75	0.21
55.11	17.53	0.21
55.11	17.49	0.11
55.12	17.76	0.21
55.13	17.84	0.21
55.13	17.66	0.21
55.14	17.31	0.21
55.14	17.42	0.22
55.15	17.60	0.11
55.15	17.52	0.21
55.16	17.38	0.21
55.16	17.75	0.21
55.17	17.78	0.21
55.17	17.60	0.21
55.18	17.59	0.21
55.18	17.80	0.21
55.18	17.60	0.21
55.18	17.67	0.21
55.21	18.09	0.21
55.21	16.75	0.20

(Continued)

TABLE 9.1 (Continued)

Age (Ma)	$\delta^{34}S$ Barite	Error (±)
55.21	17.88	0.21
55.21	18.25	0.11
55.22	18.58	0.11
55.22	17.90	0.11
55.22	18.31	0.21
55.22	17.95	0.21
55.23	18.19	0.21
55.23	18.95	0.11
55.24	17.77	0.11
55.24	17.54	0.11
55.24	17.78	0.11
55.25	17.71	0.22
55.25	17.51	0.20
55.25	17.64	0.20
55.26	17.87	0.20
55.26	17.66	0.21
55.26	17.50	0.20
55.26	17.62	0.15
55.27	17.75	0.16
55.27	17.68	0.20
55.27	17.49	0.21
55.28	17.89	0.20
55.28	17.36	0.20
55.28	17.53	0.20
55.29	17.56	0.15
55.29	17.21	0.20
55.30	17.66	0.20
55.31	17.77	0.16
55.31	17.45	0.16
55.32	17.49	0.16
55.33	17.26	0.20
55.42	17.63	0.20
55.47	17.42	0.20
55.52	17.19	0.20
55.72	17.34	0.20
55.81	18.05	0.20
55.84	16.99	0.20

(Continued)

TABLE 9.1 (Continued)

Age (Ma)	$\delta^{34}S$ Barite	Error (±)
55.97	17.24	0.20
56.13	17.23	0.20
56.22	17.53	0.20
56.38	16.94	0.20
56.44	17.60	0.20
56.54	17.72	0.20
56.76	18.07	0.20
56.92	17.44	0.20
57.22	17.60	0.20
57.92	17.99	0.20
57.95	17.42	0.20
58.03	18.28	0.20
58.09	17.10	0.20
58.45	17.13	0.20
59.09	17.76	0.20
59.36	17.99	0.20
59.64	18.12	0.20
62.26	18.63	0.20
62.46	19.04	0.20
62.55	19.05	0.20
62.56	19.37	0.20
63.91	19.38	0.20
64.06	19.00	0.20
64.26	18.96	0.20
64.37	19.04	0.20
64.62	19.00	0.20
64.74	19.14	0.20
64.80	18.93	0.20
65.02	19.30	0.20
65.21	18.95	0.30
65.27	18.94	0.30
65.57	19.11	0.30
66.06	18.76	0.30
66.80	18.80	0.30
68.72	18.88	0.27
70.08	18.82	0.30
71.40	19.09	0.30

(Continued)

TABLE 9.1 (Continued)

Age (Ma)	$\delta^{34}S$ Barite	Error (±)
73.09	19.20	0.30
74.27	19.14	0.30
74.48	19.35	0.23
75.40	19.40	0.30
75.69	19.30	0.30
76.49	19.15	0.25
78.45	18.95	0.30
78.79	19.14	0.30
80.35	19.11	0.25
81.98	19.14	0.25
83.01	18.24	0.30
83.62	18.43	0.25
83.68	18.28	0.25
83.83	18.16	0.23
85.16	18.35	0.23
87.93	18.17	0.30
90.72	18.59	0.25
92.91	18.90	0.30

(*Continued*)

TABLE 9.1 (Continued)

Age (Ma)	$\delta^{34}S$ Barite	Error (±)
93.02	17.32	0.20
93.35	18.42	0.25
93.46	19.04	0.30
93.57	18.84	0.30
93.79	19.02	0.30
95.00	18.92	0.23
95.78	19.04	0.25
97.00	18.81	0.25
98.87	17.86	0.27
100.00	16.27	0.23
101.01	15.65	0.20
102.02	15.42	0.20
103.04	15.48	0.20
104.06	15.61	0.30
107.10	15.65	0.30
108.12	15.92	0.30
109.14	16.16	0.25
110.15	15.35	0.23

(*Continued*)

TABLE 9.1 (Continued)

Age (Ma)	$\delta^{34}S$ Barite	Error (±)
111.27	16.09	0.30
111.68	16.33	0.30
112.08	16.14	0.30
112.18	15.77	0.28
112.90	16.20	0.25
113.26	15.35	0.30
115.03	15.50	0.30
115.05	15.79	0.27
115.23	15.34	0.30
115.36	15.30	0.25
117.27	15.32	0.23
117.39	16.40	0.30
117.52	16.55	0.25
117.82	18.70	0.30
117.95	17.83	0.30
119.25	19.21	0.27
120.60	19.56	0.25
121.80	19.95	0.23
124.65	20.05	0.25

this time interval making it difficult to correlate to other sites such as Site 1267 in the South Atlantic. At both Sites, however, a minimum in the $\delta^{34}S$ record was recorded and used to align the two records. Ages were determined by biostratigraphy.

S isotopes data are becoming more widely available for many study locations and, as illustrated previously, have the potential to become a more useful tool for stratigraphy and correlation as we refine the global S isotope record. The challenge in the next few years is to expand the data available to produce a reliable, high-resolution, secular data of seawater S isotope values set such that a high-resolution curve like the one currently available for the past 130 Ma could be produced and used for age determination.

Bibliography

Algeo, T.J., Ellwood, B.B., Thoa, N.T.K., Rowe, H., and Maynard, J.B., 2007, The Permian-Triassic boundary at Nhi Tao, Vietnam; evidence for recurrent influx of sulfidic watermasses to a shallow-marine carbonate platform. *Palaeogeography, Palaeoclimatology, Palaeoecology*, **252**: 304–327.

Arthur, M.A., 2000, Volcanic contributions to the carbon and sulfur geochemical cycles and global change. *In* Sigurdsson, H. (ed), *Encyclopedia of Volcanoes*. San Diego, CA: Academic Press, p. 1045–1056.

Ault, W., and Jensen, M.L., 1963, A summary of sulfur isotope standards. *In* Jensen, M.L. (ed), Biogeochemistry of Sulfur Isotopes, National Science Foundation Symposium Proceedings, Yale University, p. 16–29.

Bernasconi, S.M., Meier, I., Wohlwend, S., Brack, P., Hochuli, P.A., Bläsi, H., et al., 2017, An evaporite-based high-resolution sulfur isotope record of Late Permian and Triassic seawater sulfate. *Geochimica et Cosmochimica Acta*, **204**: 331–349.

Berner, R.A., 1999, Atmospheric oxygen over Phanerozoic time. *Proceedings of the National Academy of Sciences of the United States of America*, **96**: 10955–10957.

Berner, E.K., and Berner, R.A., 1987, *The Global Water Cycle; Geochemistry and Environment*. Englewood Cliffs, NJ: Prentice-Hall, pp 397.

Berner, R.A., and Canfield, D.E., 1989, A new model for atmospheric oxygen over Phanerozoic time. *American Journal of Science*, **289**: 333–361.

Berner, R.A., and Canfield, D.E., 1999, Atmospheric oxygen over Phanerozoic time. Proceedings of the National Academy of Sciences of the United States of America, **96**: 10955–10957.

Boersma, A., and Shackleton, N., 1977. *36*. Oxygen and carbon isotope record through the Oligocene, DSDP Site 366, Equatorial Atlantic, *In Initial Reports of the Deep Sea Drilling Project, Vol. 41*. Texas A & M University, Ocean Drilling Program, College Station, TX, pp. 957–962.

Bottrell, S.H., and Newton, R.J., 2006, Reconstruction of changes in global sulfur cycling from marine sulfate isotopes. *Earth-Science Reviews*, **75**: 59–83.

Burdett, J.W., Arthur, M.A., and Richardson, M., 1989, A Neogene seawater sulfur isotope age curve from calcareous pelagic microfossils. *Earth and Planetary Science Letters*, **94**: 189–198.

Canfield, D.E., 2001, Isotope fractionation by natural populations of sulfate-reducing bacteria. *Geochimica et Cosmochimica Acta*, **65**: 1117–1124.

Canfield, D.E., and Farquhar, J., 2009. Animal evolution, bioturbation, and the sulfate concentration of the oceans. Proceedings of the National Academy of Sciences of the United States of America **106**: 8123–8127.

Canfield, D., and Thamdrup, B., 1994, The production of ^{34}S-depleted sulfide during bacterial disproportionation of elemental sulfur. *Science*, **266**: 1973–1975.

Chiba, H., and Sakai, H., 1985, Oxygen isotope exchange rate between dissolved sulfate and water at hydrothermal temperatures. *Geochimica et Cosmochimica Acta*, **49** (4), 993–1000.

Claypool, G.E., Holser, W.T., Kaplan, I.R., Sakai, H., and Zak, I., 1980, The age curves of sulfur and oxygen isotopes in marine sulfate and their mutual interpretation. *Chemical Geology*, **28**: 199–260.

Cortecci, G., Reyes, E., Berti, G., and Casati, P., 1981, Sulfur and oxygen isotopes in Italian marine sulfates of Permian and Triassic ages. *Chemical Geology*, **34**: 65–79.

Couture, R., Miller, R.S., Gieskes, J.M., 1977. 32. Interstitial water and mineralogical studies, Leg 41, *In* Gardner J., Herring J. (Eds.), *Initial Reports of the Deep Sea Drilling Project, Vol. 41*. College Station, TX, pp. 907–914.

Crockford, P.W., et al., 2019, Claypool continued: Extending the isotopic record of sedimentary sulfate. *Chemical Geology*, **513**: 200–225.

Das, N., Horita, J., and Holland, H.D., 1990, Chemistry of fluid inclusions in halite from the Salina Group of the Michigan Basin: implications for Late Silurian Seawater and the origin of sedimentary brines. *Geochimica et Cosmochimica Acta*, **54**: 319–327.

DeBond, N., Oakes, R.L., Paytan, A., and Wortmann, U.G., 2012, Early Aptian carbon and sulphur isotope signatures at ODP Site 765. *Isotopes in Environmental and Health Studies*, **48**: 180–194.

Eagle, M., Paytan, A., Arrigo, K.R., van Dijken, G., and Murray, R.W., 2003, A comparison between excess barium and barite as indicators of carbon export. *Paleoceanography*, **18**: 1–13.

Farquhar, J., and Wing, B., 2003, Multiple sulfur isotopes and the evolution of the Earth's atmosphere. *Earth and Planetary Science Letters*, **213**: 1–13.

Farquhar, J., Bao, H., and Thiemens, M., 2000, Atmospheric influence of Earth's earliest sulfur cycle. *Science*, **289**: 756–758.

Fox, J.S., and Videtich, P.E., 1997, Revised estimate of δ^{34}S for marine sulfates from the Upper Ordovician: data from the Williston Basin, North Dakota, USA. *Applied Geochemistry*, **12**: 97–103.

Gill, B.C., Lyons, T.W., and Saltzman, M.R., 2007, Parallel, high-resolution carbon and sulfur isotope records of the evolving Paleozoic marine sulfur reservoir. *Palaeogeography, Palaeoclimatology, Palaeoecology*, **256**: 156–173.

Gill, B.C., Lyons, T.W., and Jenkyns, H.C., 2011, A global perturbation to the sulfur cycle during the Toarcian Oceanic Anoxic Event. *Earth and Planetary Science Letters*, **312**: 484–496.

Goldberg, T., Poulton, S.W., and Strauss, H., 2005, Sulphur and oxygen isotope signatures of late Neoproterozoic to early Cambrian sulphate, Yangtze Platform, China: diagenetic constraints and seawater evolution. *Precambrian Research*, **137**: 223–241.

Goldhaber, M.B., and Kaplan, I.R., 1974, The sulfur cycle. *In* Goldberg, E.D. (ed), *The Sea. 5. Marine Chemistry*. New York: Wiley, p. 569–655.

Gorjan, P., Kaiho, K., Kakegawa, T., Niitsuma, S., Chen, Z.Q., Kajiwara, Y., et al., 2007, Paleoredox, biotic and sulfur-isotopic changes associated with the end-Permian mass extinction in the western Tethys. *Chemical Geology*, **244**: 483–492.

Habicht, K.S., Canfield, D.E., and Rethmeier, J., 1998, Sulfur isotope fractionation during bacterial reduction and disproportionation of thiosulfate and sulfite. *Geochimica et Cosmochimica Acta*, **62**: 2585–2595.

Habicht, K.S., Gade, M., Thamdrup, B., Berg, P., and Canfield, D.E., 2002, Calibration of Sulfate Levels in the Archean Ocean. *Science*, **298**: 2372–2374.

Harland, W.B., Armstrong, R.L., Cox, A.V., Craig, L.A., Smith, A.G., and Smith, D.G., 1990, *A Geologic Time Scale 1989*. Cambridge: Cambridge University Press, pp 263.

Holser, W.T., and Kaplan, I.R., 1966, Isotope geochemistry of sedimentary sulfates. *Chemical Geology*, **1**: 93–135.

Holser, W.T., Schidlowski, M., Mackenzie, F.T., and Maynard, J.B., 1988, Geochemical cycles of carbon and sulfur. *In* Gregor, C.B., Garrels, R.M., Mackenzie, F.T., and Maynard, J.B. (eds), *Chemical Cycles in the Evolution of the Earth*. New York: Wiley, p. 105–173.

Horita, J., Zimmermann, H., and Holland, H.D., 2002, Chemical evolution of seawater during the Phanerozoic; implications from the record of marine evaporites. *Geochimica et Cosmochimica Acta*, **66**: 3733–3756.

Hough, M.L., Shields, G.A., Evins, L.Z., Strauss, H., Henderson, R.A., and Mackenzie, S., 2006, A major sulphur isotope event at c. 510Ma: a possible anoxia-extinction-volcanism connection during the Early-Middle Cambrian transition? *Terra Nova*, **18**: 257–263.

Hurtgen, M.T., Arthur, M.A., Suits, N.S., and Kaufman, A.J., 2002, The sulfur isotopic composition of Neoproterozoic seawater sulfate: implications for a snowball Earth? *Earth and Planetary Science Letters*, **203**: 413–429.

Hurtgen, M.T., Pruss, S.B., and Knoll, A.H., 2009, Evaluating the relationship between the carbon and sulfur cycles in the later Cambrian ocean: an example from the Port au Port Group, western Newfoundland, Canada. *Earth and Planetary Science Letters*, **281**: 288–297.

Jenkyns, H.C., 1988, The early Toarcian (Jurassic) anoxic event – stratigraphic, sedimentary, and geochemical evidence. *American Journal of Science*, **288**: 101–151.

Jenkyns, H.C., 2010, Geochemistry of oceanic anoxic events. *Geochemistry, Geophysics, Geosystems*, **11**: Q03004.

Johnston, D.T., 2011, Multiple sulfur isotopes and the evolution of Earth's surface sulfur cycle. *Earth-Science Reviews*, **106**: 161–183.

Kah, L.C., Lyons, T.W., and Frank, T.D., 2004, Low marine sulphate and protracted oxygenation of the Proterozoic biospheres. *Nature*, **431**: 834–838.

Kah, L.C., Thompson, C.K., Henderson, M.A., and Zhan, R., 2016, Behavior of marine sulfur in the Ordovician. *Palaeogeography, Palaeoclimatology, Palaeoecology*, **458**: 133–153.

Kampschulte, A., and Strauss, H., 2004, The sulfur isotopic evolution of Phanerozoic sea water based on the analysis of structurally substituted sulfate in carbonates. *Chemical Geology*, **204**: 255–286.

Kampschulte, A., Buhl, D., and Strauss, H., 1998, The sulfur and strontium isotopic compositions of Permian evaporites from the Zechstein basin, northern Germany. *Geologische Rundschau*, **87**: 192–199.

Kampschulte, A., Bruckschen, P., and Strauss, H., 2001, The sulphur isotopic composition of trace sulphates in Carboniferous brachiopods: implications for coeval seawater, correlation with other geochemical cycles and isotope stratigraphy. *Chemical Geology*, **175**: 149–173.

Kaplan, I.R., 1983, Stable isotopes of sulfur, nitrogen and deuterium in recent marine environments. Stable Isotopes in Sedimentary Geology, Chap. 2: 108 pp. *In* Arthur, M.A., Anderson, T.F., Kaplan, I.R., Veizer, J., and Land, L.S. (eds), Stable Isotopes in Sedimentary Geology. *SEPM Short Course Notes,* Vol. 10.

Kaplan, I.R., Emery, K.O., and Rittenberg, S.C., 1963, The distribution and isotopic abundance of sulphur in recent marine sediments off southern California. *Geochimica et Cosmochimica Acta*, **27**: 297–331.

Kramm, U., and Wedepohl, K.H., 1991, The isotopic composition of strontium and sulfur in seawater of Late Permian (Zechstein) age. *Chemical Geology*, **90**: 253–262.

Krouse, H.R., 1980, Sulphur isotopes in our environment. *In* Fritz, P., and Fontes, J.C. (eds), *Handbook of Environmental Isotope Geochemistry*. Amsterdam: Elsevier, p. 435–471.

Lancelot, Y., Seibold, E., Cepek, P., Dean, W.E., Eremeev, V., Gardner, J., et al., 1977. Site 366: Sierra Leone Rise, *In Initial Reports of the Deep Sea Drilling Project, 41*. United States Government Printing Office, Washington, DC, pp. 121–161.

Langton, S.J., Rabideaux, N.M., Borrelli, C., and Katz, M.E., 2016, South-eastern Atlantic deep-water evolution during the late-middle Eocene to earliest Oligocene (Ocean Drilling Program Site 1263 and Deep Sea Drilling Project Site 366). *Geosphere*, **12**: 103–1047.

Longinelli, A., and Flora, O., 2007, Isotopic composition of gypsum samples of Permian and Triassic age from the north-eastern Italian Alps: palaeoenvironmental implications. *Chemical Geology*, **245**: 275–284.

Lowenstein, T.K., Timofeeff, M.N., Brennan, S.T., Hardie, L.A., and Demicco, R.V., 2001, Oscillations in Phanerozoic seawater chemistry; evidence from fluid inclusions. *Science*, **294**: 1086–1088.

Luo, G., Kump, L.R., Wang, Y., Tong, J., Arthur, M.A., Yang, H., et al., 2010, Isotopic evidence for an anomalously low oceanic sulfate concentration following End-Permian Mass Extinction. *Earth and Planetary Science Letters*, **300**: 101–111.

Lyons, T.W., Walter, L.M., Gellatly, A.M., Martini, A.M., and Blake, R. E., 2004, Sites of anomalous organic remineralization in the carbonate sediments of South Florida, USA; the sulfur cycle and carbonate-associated sulfate. *Geological Society of America Special Papers*, **379**: 161–176.

Markovic, S., Paytan, A., and Wortmann, U.G., 2015, Pleistocene sediment offloading and the global sulfur cycle. *Biogeosciences*, **12**: 3043–3060.

Markovic, S., Paytan, A., Li, H., and Wortmann, U.G., 2016, A revised seawater sulfate oxygen isotope record for the last 4Myr. *Geochimica et Cosmochimica Acta*, **175**: 239–251.

Mazumdar, A., and Strauss, H., 2006, Sulfur and strontium isotopic compositions of carbonate and evaporite rocks from the late Neoproterozoic-early Cambrian Bilara Group (Nagaur-Ganganagar Basin, India): constraints on intrabasinal correlation and global sulfur cycle. *Precambrian Research*, **149**: 217–230.

McArthur, J.M., Howarth, R.J., and Bailey, T.R., 2001, Strontium isotope stratigraphy: LOWESS Version 3. Best-fit line to the marine Sr-isotope curve for 0 to 509Ma and accompanying look-up table for deriving numerical age. *Journal of Geology*, **109**: 155–169.

Misi, A., Kaufman, A.J., Veizer, J., Powis, K., Azmy, K., Boggiani, P.C., et al., 2007, Chemostratigraphic correlation of Neoproterozoic successions in South America. *Chemical Geology*, **237**: 143–167.

Newton, R.J., Pevitt, E.L., Wignal, P.B., and Bottrell, S.H., 2004, Large shifts in the isotopic composition of seawater sulphate across the Permo-Triassic boundary in northern Italy. *Earth and Planetary Science Letters*, **218**: 331–345.

Newton, R.J., Reeves, E.P., Kafousia, N., Wignall, P.B., Bottrell, S.H., and Sha, J.-G., 2011, Low marine sulfate concentrations and the isolation of the European epicontinental sea during the Early Jurassic. *Geology*, **39**: 7–10.

Nunes, F., and Norris R.D., 2005, Data report: High-resolution stable isotope records across the Paleocene/Eocene boundary, ODP Sites 1220 and 1221. *In* Wilson, P.A., Lyle, M., Firth, J.V. (eds.), Proceedings of the Ocean Drilling Program, Scientific Results, Vol. 199. College Station, TX, pp. 1–12.

Ohkouchi, N., Kawamura, K., Kajiwara, Y., Wada, E., Okada, M., Kanamatsu, T., et al., 1999, Sulfur isotope records around Livello Bonarelli (Northern Apennines, Italy) black shale at the Cenomanian-Turonian boundary. *Geology*, **27**: 535–538.

Orti, F., Rosell, L., and Anadón, P., 2010, Diagenetic gypsum related to sulfur deposits in evaporites (Libros Gypsum, Miocene, NE Spain). *Sedimentary Geology*, **228**: 304–318.

Paytan, A., Kastner, M., Martin, E.E., Macdougall, J.D., and Herbert, T., 1993, Marine barite as a monitor of seawater strontium isotope composition. *Nature*, **366**: 45–49.

Paytan, A., Kastner, M., Campbell, D., and Thiemens, M.H., 1998, Sulfur isotopic composition of Cenozoic seawater sulfate. *Science*, **282**: 1459–1462.

Paytan, A., Kastner, M., Campbell, D., and Thiemens, M.H., 2004, Seawater sulfur isotope fluctuations in the cretaceous. *Science*, **304**: 1663–1665.

Paytan, A., Gray, E.T., Ma, Z., Erhardt, A., and Faul, A., 2011, Application of sulphur isotopes for stratigraphic correlation. *Isotopes in Environmental and Health Studies*, **48**: 195–206.

Peryt, T.M., Halas, S., Kovalevych, V.M., Petrychenko, Y., and Dzhinoridze, N.M., 2005, The sulphur and oxygen isotopic composition of Lower Cambrian anhydrites in East Siberia. *Geological Quarterly*, **49**: 235–242.

Pierre, C., and Rouchy, J.M., 1986, — Oxygen and sulfur isotopes in anhydrites from Givetian and Visean evaporites of Northern France and Belgium. *Chemical Geology (Isotope Geoscience section)*, **58**: 245–252.

Planavsky, N.J., Bekker, A., Hofmann, A., Owens, J.D., and Lyons, T. W., 2012, Sulfur record of rising and falling marine oxygen and

sulfate levels during the Lomagundi event. *Proceedings of the National Academy of Sciences of the United States of America*, **109**: 18300–18305.

Pokrovskii, B.G., Melezhik, V.A., and Bujakaite, M.I., 2006, Carbon, oxygen, strontium, and sulfur isotopic compositions in late Precambrian rocks of the Patom Complex, central Siberia; Communication 2, Nature of carbonates with ultralow and ultrahigh $\delta^{13}C$ values. *Lithology and Mineral Resources*, **41**: 576–587.

Present, T.M., Paris, G., Burke, A., Fischer, W.W., and Adkins, J.F., 2015, Large carbonate associated sulfate isotopic variability between brachiopods, micrite, and other sedimentary components in Late Ordovician strata. *Earth and Planetary Science Letters*, **432**: 187–198.

Rees, C.E., Jenkins, W.F., and Monster, J., 1978, The sulphur isotopic composition of ocean water sulphate. *Geochimica et Cosmochimica Acta*, **42**: 377–382.

Rennie, V.C.F., Paris, G., Sessions, A.L., Abramovich, A., Turchyn, A. V., and Adkins, J.F., 2018, Cenozoic record of $\delta^{34}S$ in foraminiferal calcite implies an early Eocene shift to deep-ocean sulfide burial. *Nature Geoscience*, **11**: 761–765.

Rick, B., 1990, Sulphur and oxygen isotopic composition of Swiss Gipskeuper (Upper Triassic). *Chemical Geology: Isotope Geoscience Section*, **80**: 243–250.

Sakai, H., 1972, Oxygen isotopic ratios of some evaporites from Precambrian to Recent ages. *Earth and Planetary Science Letters*, **15**: 201–205.

Schobben, M., Stebbins, A., Algeo, T.J., Strauss, H., Leda, L., Haas, J., et al., 2017, Volatile earliest Triassic sulfur cycle: a consequence of persistent low seawater sulfate concentrations and a high sulfur cycle turnover rate? *Palaeogeography, Palaeoclimatology, Palaeoecology*, **486**: 74–85.

Scholle, P.A., 1995, Carbon and sulfur isotope stratigraphy of the Permian and adjacent intervals. *In* Scholle, P.A., Peryt, T.M., and Ulmer-Scholle, D.S. (eds), *The Permian of northern Pangea. Vol. 1*. Berlin: Springer-Verlag, p. 133–149.

Scott, C., Wing, B.A., Bekker, A., Planavsky, N.J., Medvedev, P., Bates, S.M., et al., 2014, Pyrite multiple-sulfur isotope evidence for rapid expansion and contraction of the early Paleoproterozoic seawater sulfate reservoir. *Earth and Planetary Science Letters*, **389**: 95–104.

Sim, M.S., Ono, S., and Hurtgen, M.T., 2015, Sulfur isotope evidence for low and fluctuating sulfate levels in the Late Devonian ocean and the potential link with the mass extinction event. *Earth and Planetary Science Letters*, **419**: 52–62.

Song, H.Y., Tong, J.N., Algeo, T.J., Song, H.J., Qiu, H.O., Zhu, Y.Y., et al., 2014, Early Triassic seawater sulfate drawdown. *Geochimica et Cosmochimica Acta*, **128**: 95–113.

Strauss, H., 1993, The sulfur isotopic record of Precambrian sulfates; new data and a critical evaluation of the existing record. *Precambrian Research*, **63**: 225–246.

Strauss, H., 1997, The isotopic composition of sedimentary sulfur through time. *Palaeogeography, Palaeoclimatology, Palaeoecology*, **132**: 97–118.

Strauss, H., Banerjee, D.M., and Kumar, V., 2001, The sulfur isotopic composition of Neoproterozoic to early Cambrian seawater – evidence from the cyclic Hanseran evaporites, NW India. *Chemical Geology*, **175**: 17–28.

Surakotra, N., Promkotra, S., Charusiri, P., Maruoka, T., and Hisada, K. I., 2018, Sulfur, Strontium, Carbon, and Oxygen Isotopes of Calcium Sulfate Deposits in Late Carboniferous Rocks of the Loei-Wang Saphung (LWS) Area, Loei Province, Thailand. *Geosciences*, **8**: 229–239.

Thode, H.G., and Monster, J., 1965, Sulfur-isotope geochemistry of petroleum, evaporites, and ancient seas. *American Association of Petroleum Geologists Memoir*, **4**: 367–377.

Thompson, C.K., and Kah, L.C., 2012, Sulfur isotope evidence for widespread euxinia and a fluctuating oxycline in Early to Middle Ordovician greenhouse oceans. *Palaeogeography, Palaeoclimatology, Palaeoecology*, **313-314**: 189–214.

Turchyn, A.V., Schrag, D.P., Coccioni, R., and Montanari, A., 2009, Stable isotope analysis of the Cretaceous sulfur cycle. *Earth and Planetary Science Letters*, **285**: 115–123.

Ueda, A., Campbell, F.A., Krouse, H.R., and Spencer, R.J., 1987, $^{34}S/^{32}S$ variations in trace sulphide and sulphate in carbonate rocks of a Devonian reef, Alberta, Canada, and the Precambrian Siyeh Formation, Montana, USA. *Chemical Geology: Isotope Geoscience Section*, **65**: 383–390.

Utrilla, R., Pierre, C., Orti, F., and Pueyo, J.J., 1992, Oxygen and sulphur isotope compositions as indicators of the origin of Mesozoic and Cenozoic evaporites from Spain. *Chemical Geology*, **102**: 229–244.

Walter, M.R., Veevers, J.J., Calver, C.R., Gorjan, P., and Hill, A.C., 2000, Dating the 840-544 Ma Neoproterozoic interval by isotopes of strontium, carbon, sulfur in seawater, and some interpretative models. *Precambrian Research*, **100**: 371–433.

Williford, K.H., Foriel, J., Ward, P.D., and Steig, E.J., 2009, Major perturbation in sulfur cycling at the Triassic-Jurassic boundary. *Geology*, **37**: 835–838.

Worden, R.H., Smalley, P.C., and Fallick, A.E., 1997, Sulfur cycle in buried evaporites. *Geology*, **25**: 643–646.

Wotte, T., Strauss, H., Fugmann, A., and Garbe-Schönberg, D., 2012, Paired $\delta^{34}S$ data from carbonate-associated sulfate and chromium-reducible sulfur across the traditional Lower-Middle Cambrian boundary of W-Gondwana. *Geochimica et Cosmochimica Acta*, **85**: 228–253.

Wu, N.P., Farquhar, J., Strauss, H., Kim, S.-T., and Canfield, D.E., 2010, Evaluating the S-isotope fractionation associated with Phanerozoic pyrite burial. *Geochimica et Cosmochimica Acta*, **74** (7), 2053–2071, https://doi.org/10.1016/j.gca.2009.12.012.

Wu, N.P., Farquhar, J., and Strauss, H., 2014, $\delta^{34}S$ and $\Delta^{33}S$ records of Paleozoic seawater sulfate based on the analysis of carbonate associated sulfate. *Earth and Planetary Science Letters*, **399**: 44–51, https://doi.org/10.1016/j.epsl.2014. 05.004.

Yao, W.Q., Paytan, A., and Wortmann, U.G., 2018, Large-scale ocean deoxygenation during the Paleocene-Eocene Thermal Maximum. *Science*, **361**: 804–806.

Yao, W.Q., Wortmann, U.G., and Paytan, A., 2019, Sulfur isotopes – Use for stratigraphy during times of rapid perturbations. *Stratigraphy & Timescales*, **4**: 1–33.

Yao, W.Q., Paytan, A., Griffith, E.M., Martínez-Ruiz, F., Markovic, S., and Wortmann, U.G., 2020, A revised seawater sulfate S-isotope curve for the Eocene. *Chemical Geology*, **532**.